JOUR. FAC. SCI., SHINSHU UNIV. Vol. 2, No. 1, pp. 19—85, June. 1967

*Electronic Specific Heat and Magnetic Susceptibility of Transition Metals and Alloys**

By ATSUSHI KATSUKI

Department of Physics, Faculty of Science,
Shinshu University
(Received June 30, 1967)

Abstract

Electronic specific heats, C_E, of transition metals are estimated from observed specific heat data. It is shown that for some transition metals which should be called "plus group" metals, $C_E > \gamma(0)\,T$ where $\gamma(0)$ is the value of C_E/T at very low temperatures, whereas for other metals which should be called "minus group" metals, $C_E < \gamma(0)\,T$. The formulae for Pauli paramagnetic susceptibility, χ_0, electronic specific heat coefficient, γ, and their field dependences are given. The density of states curves are determined from specific heat data at very low temperatures of some series of transition metals and their alloys on the basis of the rigid band model. By making use of these density of states curves, electronic specific heats and the Pauli paramagnetic susceptibilities are calculated. Comparing the calculated results of χ_0 and observed magnetic susceptibilities χ, we estimate the molecular field coefficients α and the orbital paramagnetic susceptibilities $\chi_{\text{orb.}}$ for the transition metals and their alloys. The NMR shift of V^{51} in V–Cr alloys and of Nb^{93} and Tc^{99} in Nb–Mo and Nb–Tc alloys are explained by making use of the estimated values of $\chi_{\text{orb.}}$ and α. STONER's condition of ferromagnetism is examined and it is pointed out that STONER's condition is a sufficient condition of ferromagnetism for the electrons in the band, but is not always a necessary one.

§ 1 Introduction

It is well known that in some transition metals the magnetic susceptibilities increase with increasing temperature ($d\chi/dT > 0$), whereas in others they decrease with increasing temperature ($d\chi/dT < 0$). In general, the values of magnetic susceptibilities, χ, and temperature coefficients of electronic specific heats, $\gamma\,(\equiv C_E/T)$, are small in the former metals and large in the later metals.[1] We will call the former metals "*plus group*" and the later ones "*minus group*" hereafter.

* Thesis, Nagoya University, 1965.

Table 1 Magnetic susceptibilities, electronic specific heat coefficients and their temperature dependences in transition metals.

(1) : values of χ in 10^{-4} emu/mole at room temperature.
(2) : values of $d\chi/dT$ in 10^{-8} emu/mole deg at room temperature.
(3) : values of $\gamma(0)$ in 10^{-4} cal/mole deg^2.
(4) : values of $\gamma(800°K)/\gamma(0)$.

The values of χ and $d\chi/dT$ are quoted by TAKAHASHI from the following references.

Sc, Y, La– H. BOMMER (1939) Z. Electrochem. **45**, 357; Ti– W. KLEMM (1939) Z. Electrochem. **45**, 354; Zr– 32; Hf– 1; V– 29; Nb, Mo, W– 49; Cr– T. R. McGUIRE and C. J. KRIESSMAN (1952) Phys. Rev. **85**, 452; Mn– A. SERRES (1938) J. Phys. Rad. **9**, 377; Tc– 50; Re– N. PERARKIS and L. CAPATOS (1935) J. Phys. Rad. **6**, 642; Ru, Os, Ir– A. N. GUTHER and L. T. BOURLAND (1931) Phys. Rev. **37**, 303; Rh, Pt– 22; Pd– D. GERSTENBERG (1958) Ann. Physik. **2**, 236.

The values of $\gamma(0)$ are quoted from the following references.

Sc, Y, La– 15; Ti, Hf– 14; Zr– 12, V– 10; Nb, Mo– 19; Ta, Mn, Re, Ru, Os, Ir– 23; Cr– 12; W– American Institute of Physics Handbook, 2nd edition (McGraw-Hill Book Comp., Inc., New York, 1963) 4–61; Tc– 20; Fe, Co, Ni– 17; Rh– 22; Pd– 20; Pt–24.

The values of $\gamma(800°K)/\gamma(0)$ are estimated in the present work. Values of $\gamma(1200°K)/\gamma(0)$ and $\gamma(1500°K)/\gamma(0)$ are given for Fe and Co, respectively, because the temperature of 800° K is lower than the Curie temperature of Fe and Co metals.

Letters *p* and *m* mean "plus" and "minus" group, respectively.

	(*m*)	(*p*)	(*m*)	(*p*)	(*m*)	(*p*)		(*m*)
	Sc	Ti	V	Cr	Mn	Fe	Co	Ni
(1)	3.15	1.53	2.96	1.88	5.33	—	—	—
(2)	−24	+4	−2	+1	−14	—	—	—
(3)	27.0	8.5	21.2	3.8	43	12.0	12.0	17.4
(4)	—	1.8	0.5	4.7	0.3	1.2*	1.2**	0.8
	Y	Zr	Nb	Mo	Tc	Ru	Rh	Pd
(1)	1.91	1.20	2.12	0.89	1.21	0.44	1.02	5.70
(2)	−7	+2.5	−2	+0.2	—	0	+3	−140
(3)	24.4	6.92	28	4.8	20	8.0	11.1	22.2
(4)	—	2.7	0.2	1.2	—	—	1.1	0.3
	La	Hf	Ta	W	Re	Os	Ir	Pt
(1)	1.22	0.81	1.54	0.59	0.69	0.10	0.26	1.88
(2)	−3	+1	−1	+0	0	+1	+2	−23
(3)	24.1	6.3	14.0	3.1	5.85	5.62	7.5	15.55
(4)	0.8	—	0.4	1.4	—	—	0.9	0.4

* 1200°K ** 1500°K

Transition metals in the same column of the periodic table belong to the same group and two groups adjoin each other (Table 1; Figs. 1A∼B).

An interpretation that the "plus group" metals are antiferromagnetic with high Néel temperature is unreasonable.[2] According to the band picture for d–electrons, it has been shown qualitatively that, if the Fermi level at 0°K lies at

a minimum of the density of states, then the values of χ and γ are small and χ increase with increasing temperature.[3] Some calculations of spin paramagnetic susceptibility for Cr metal, which is a typical "plus group" metal, were performed on the basis of a simplified model.[2]

If the interpretation by the band picture is adequate for d-electrons in transition metals, there should be a certain relation between temperature dependences of magnetic susceptibility and electronic specific heat. Roughly speaking, by taking the low temperature expansions of χ and γ into consideration, $d\gamma/dT$ will be positive for the "plus group" metals (for which $d\chi/dT>0$), and $d\gamma/dT$ will be negative for the "minus group" metals (for which $d\chi/dT<0$). Therefore, the values of γ at high temperatures will be larger for "plus group" and will be smaller for "minus group" than those at low temperatures, respectively.

From this point of view, we analyze the experimental data of specific heats of various transition metals and confirm the fact that in the "plus group" metals γ (high temp.) $>\gamma$ (low temp.) whereas in the "minus group" metals γ (high temp.) $<\gamma$ (low temp.) (§ 2). From this fact, we consider for the band picture of the d-electrons to be adequate for such a problem in the transition metals.

According to the band theory, there is a proportionality relation between the values of χ and γ. In real metals, however, the observed values of χ are in general considerably larger than those expected from the values of γ. STONER attributed this difference to an effect of molecular field.[1] On the other hand, it is expected that in transition metals the contribution of the orbital paramagnetism on magnetic susceptibility is comparable to that of the Pauli paramagnetism.[4] Therefore, it will be significant to investigate separately the effect of the molecular field and the contribution of the orbital paramagnetism in comparing the calculated values of the Pauli paramagnetic susceptibility, χ_0, with the observed values of χ over a wide range of temperatures. For such a discussion to be significant, it is necessary that the density of states curves used in the calculation of χ_0 are very similar to that of the real metals. Recently, systematical measurements of specific heats have been made for several series of transition metals and their alloys. From these experimental data the density of states curves are determinable for the transition metals and alloys on the basis of the rigid band model. The band forms obtained in this way are complicated and are not expressible by simple analytical functions. However, it is able by means of an electronic computer to calculate numerically the electronic specific heat, C_E, and the unenhanced spin paramagnetic susceptibility, χ_0, for the metals and alloys with complicated shapes of the density of states curve.

The values of the molecular field coefficient, α, and the orbital paramagnetic susceptibility, $\chi_{\text{orb.}}$, estimated from a comparison of calculated values of χ_0 with

observed values of χ over a wide range of temperatures will be regarded as reliable, if some physical properties — e. g., the composition dependence of NMR shift in an alloy system — are interpretable by these values of α and $\chi_{\text{orb.}}$.

In § 2, data of specific heat of transition metals are analyzed and it is shown that the relations γ (high temp.)$>\gamma$(low temp.) and γ(high temp.)$<\gamma$(low temp.) well hold, respectively, for "plus group" and "minus group" metals. Formulations of magnetic susceptibility, electronic specific heat and field dependences of them are derived in § 3. The density of states curves for b. c. c.- and f. c. c.- 3d, 4d and 5d series of transition metals and their alloys, respectively, are determined from experimental data of low temperature specific heat on the basis of the rigid band model in § 4. Calculated results of electronic specific heats and the Pauli paramagnetic susceptibilities are given in § 5. In § 6, we compare the calculated results of electronic specific heats with those estimated in § 2. The calculated results of the Pauli paramagnetic susceptibilities and the observed values of magnetic susceptibilities are compared and the contributions of the molecular field and the orbital paramagnetism are evaluated in § 7. In § 8, by taking account of the contribution from the orbital paramagnetism, interpretations are given for the composition dependences of NMR shift of V^{51}, Nb^{93} and Tc^{99} in V–Cr, Nb–Mo and Nb–Tc systems. In § 9, a consideration on the condition of ferromagnetism by the band model is done in connection with the calculations given in § 5.

§ 2 Analysis of Electronic Specific Heat

Electronic specific heat, C_E, of a transition metal is obtained from observed specific heat, C_p, as follows:

$$C_E = C_p - (C_p - C_v) - C_D, \tag{2. 1}$$

where C_v is the specific heat at constant volume and C_D is the Debye specific heat. C_D can be calculated from the known Debye temperature, Θ_D. The dilatation correction $C_p - C_v$ is written as

$$C_p - C_v = 9TV\alpha_l^2/\beta, \tag{2. 2}$$

where V, α_l and β are atomic volume, thermal expansion coefficient and compressibility, respectively. As the measurements of β as a function of temperature are lacking at present, we use the following empirical formula,[5]

$$C_p - C_v = aTC_p^2, \tag{2. 3}$$

where a is a proportionality constant determined from the values of α_l,[6] β,[7] V and

C_p at room temperature (cf. Appendix I on the validity of the approximation (2. 3)). For several transition metals the values of $C_p - C_v$, C_D, C_E obtained in this way and the values, $\gamma(0)T$ and C_p[8] observed are shown in Figs. 2A $\sim$ Q, where $\gamma(0)$ is the very low temperature value of γ. It is noticed that $C_E > \gamma(0)T$ for "plus group" metals and $C_E < \gamma(0)T$ for "minus group" metals.

Temperature variations of reduced values of γ, $\gamma^*(T)$ $(\equiv\gamma(T)/\gamma(0))$, for various transition metals are shown in Fig. 3. It is easily seen that the $\gamma^*(T)$ curves of "plus group" metals lie in the upper region of the figure and those of "minus group" metals lie in the lower region. In Table 1, the values of γ^* (800° K) are given together with the values of χ, $d\chi/dT$ and $\gamma(0)$, and it is found that γ^*(800° K) >1 for "plus group" metals and γ^* (800° K) <1 for "minus group" metals. In order to make clearly visible the relation between $\gamma(0)$, χ and γ^*, we show the values of $\gamma(0)$, χ and γ^* (800° K) in Figs. 1A$\sim$C, respectively.

It is concluded from above analysis, that the electronic specific heats of the transition metals behave as the temperature dependences of them are consistently interpretable by the band model. Therefore, it seems to be reasonable to stand on the viewpoint of the band picture, at least, for such a problem.

§ 3 Formulation

(*1*) *Basic equation*

The Pauli paramagnetic susceptibility, χ_0, and electronic specific heat, C_E, as functions of temperature and magnetic field are formulated in the case of an arbitrary density of states, $\nu(\varepsilon)$, in the following way. The total number of electrons, N_0, is given by

$$N_0 = 2\int_{\varepsilon_1}^{\zeta_0} \nu(\varepsilon)d\varepsilon, \tag{3. 1}$$

where ζ_0 is the Fermi level energy at 0°K and ε_1 is the energy at the bottom of the band. Fermi-Dirac integrals are defined as

$$\left.\begin{aligned} &F_i(\zeta) = \int_{\varepsilon_1}^{\varepsilon_2} \varepsilon^i \nu(\varepsilon) f(\varepsilon) d\varepsilon, \\ \text{and}\quad &F_i^{(n)}(\zeta) = \frac{\partial^n}{\partial \zeta^n} F_i(\zeta), \end{aligned}\right\} \tag{3. 2}$$

where ε_2 is the energy at the top of the band and $f(\varepsilon)$ is the Fermi distribution function,

$$f(\varepsilon) = 1/\left\{1 + \exp\left(\frac{\varepsilon - \zeta}{kT}\right)\right\}, \tag{3. 3}$$

where ζ is the Fermi level at the temperature T. Then, the numbers of the electrons with plus- and minus-spin at the temperature T under magnetic field H are given, respectively, by

$$N_{\pm} = F_0(\zeta_T + \Delta\zeta \pm \mu H), \tag{3.4}$$

and

$$N_+ + N_- = N_0, \tag{3.5}$$

where μ is the Bohr magneton and $\Delta\zeta$ is the shift of the Fermi level ζ_T due to the magnetic field H. When $H = 0$, ζ_T satisfies the relation,

$$F_0(\zeta_T) - \frac{N_0}{2} = 0. \tag{3.6}$$

Assuming $\mu H << kT$ and expanding $N_{\pm}$ in terms of H, we obtain, up to the power of H^2,

$$\Delta\zeta = -(1/2)\frac{F_0^{(2)}(\zeta_T)}{F_0^{(1)}(\zeta_T)}(\mu H)^2. \tag{3.7}$$

(2) *Magnetic susceptibility*

Magnetization is given by

$$M = \mu(N_+ - N_-). \tag{3.8}$$

Assuming $\mu H << kT$ and expanding $N_{\pm}$ in terms of H, we obtain up to the power of H^3,

$$\mathrm{M} = 2\mu^2 F_0^{(1)} H + \mu^4 \left\{\frac{F_0^{(3)}}{3} - \frac{(F_0^{(2)})^2}{F_0^{(1)}}\right\} H^3. \tag{3.9}$$

Then, the Pauli paramagnetic susceptibility, χ_0, is written as

$$\chi_0(T, H) \equiv \frac{dM}{dH} = \chi_0(T)(1 + BH^2), \tag{3.10}$$

where

$$\chi_0(T) = 2\mu^2 F_0^{(1)}, \tag{3.11}$$

and

$$B = \frac{\mu^2}{2}\left\{\frac{F_0^{(3)}}{F_0^{(1)}} - 3\left(\frac{F_0^{(2)}}{F_0^{(1)}}\right)^2\right\}. \tag{3.12}$$

(3) *Electronic specific heat*

At the temperature T and under magnetic field H, the total energy of electrons is

$$E = F_1(\zeta_T + \Delta\zeta + \mu H) + F_1(\zeta_T + \Delta\zeta - \mu H) - \mu H(N_+ - N_-), \tag{3.13}$$

where the first and second terms are the "kinetic" energy of plus-and minus-spin electrons, respectively, and the third term is the magnetic energy. Assuming $\mu H << kT$ and expanding E in terms of H, we obtain up to the power of H^2,

$$E = 2F_1 + \left\{ -\frac{F_0^{(2)}F_1^{(1)}}{F_0^{(1)}} + F_1^{(2)} - 2F_0^{(1)} \right\}(\mu H)^2. \tag{3.14}$$

Then, the electronic specific heat is given by

$$C_E(T, H) \equiv \frac{dE}{dT} = C_E(T)(1 + DH^2), \tag{3.15}$$

where

$$C_E(T) \equiv \gamma(T)T = \frac{2}{T}\left\{ F_2^{(1)} - \frac{(F_1^{(1)})^2}{F_0^{(1)}} \right\}, \tag{3.16}$$

and

$$D = \frac{\mu^2}{C_E(T)T}\left\{ 2F_0^{(1)} - 4\left(F_1^{(2)} - \frac{F_0^{(2)}F_1^{(1)}}{F_0^{(1)}} \right) + F_2^{(3)} - \frac{2F_1^{(1)}F_1^{(3)} + F_0^{(2)}F_2^{(2)}}{F_0^{(1)}} + \frac{2F_0^{(2)}F_1^{(1)}F_1^{(2)} + F_0^{(3)}(F_1^{(1)})^2}{(F_0^{(1)})^2} - \frac{(F_0^{(2)}F_1^{(1)})^2}{(F_0^{(1)})^3} \right\}. \tag{3.17}$$

In equations (3.9), (3.11), (3.12), (3.14), (3.16) and (3.17), $F_i^{(n)}(\zeta_T)$ is written as $F_i^{(n)}$ for the sake of simplicity.

(4) *Low temperature expansion etc.*

At low temperatures, expanding $\chi_0(T)$ and $\gamma(T)$ $(\equiv C_E(T)/T)$ in terms of T, we obtain up to the power of T^2,

$$\chi_0(T) = \chi_0(0)\left\{ 1 + \frac{\pi^2}{6}\left\{ \frac{\nu''(\zeta_0)}{\nu(\zeta_0)} - \left(\frac{\nu'(\zeta_0)}{\nu(\zeta_0)} \right)^2 \right\}(kT)^2, \right. \tag{3.11'}$$

and

$$\gamma(T)=\gamma(0)\left[1+\frac{\pi^2}{2}\left\{\frac{7}{5}\frac{\nu''(\zeta_0)}{\nu(\zeta_0)}-\left(\frac{\nu'(\zeta_0)}{\nu(\zeta_0)}\right)^2\right\}(kT)^2\right], \tag{3.16'}$$

where

$$\chi_0(0)=2\mu^2\nu(\zeta_0), \tag{3.18}$$

$$\gamma(0)=\frac{2}{3}\pi^2k^2\nu(\zeta_0), \tag{3.19}$$

and

$$\nu^{(n)}(\zeta_0)=(d^n\nu(\varepsilon)/d\varepsilon^n)_{\varepsilon=\zeta_0}.$$

If the Fermi level ζ_0 lies at a minimum of the density of states curve, then the temperature coefficients of χ_0 and γ are positive in a temperature range where the expansions (3.11') and (3.16') are valid. Even if ζ_0 is not at a minimum density of states, if the curvature of the density of states curve at ζ_0 is positive and large enough, then the temperature coefficients of χ_0 and γ can be positive. Therefore, it is expected that a maximum exists in the temperature dependences of χ_0 and γ, if the Fermi level is in the vicinity of a peak and there the density of states curve is concave enough upwards. In a temperature range where the expansion are valid, if the temperature coefficient of χ_0 is positive, then also that of γ is necessarily positive (from this fact we have guessed that a metal with positive value of $d\chi/dT$ has also positive value of $d\gamma/dT$) and if that of γ is negative, then also that of χ_0 is necessarily negative.

Formulae (3.11) and (3.16) for χ_0 and γ are transformed as follows :

$$\chi_0(T)=-2\mu^2\int\nu(\varepsilon)f'(\varepsilon)d\varepsilon, \tag{3.11''}$$

and

$$\gamma(T)=-\frac{2}{T^2}\left[\int\varepsilon^2\nu(\varepsilon)f'(\varepsilon)d\varepsilon-\frac{\left\{\int\varepsilon\nu(\varepsilon)f'(\varepsilon)d\varepsilon\right\}^2}{\int\nu(\varepsilon)f'(\varepsilon)d\varepsilon}\right], \tag{3.16''}$$

where,

$$f'(\varepsilon)\equiv\frac{\partial f(\varepsilon)}{\partial\varepsilon}=-\frac{1}{kT}\frac{\exp\frac{\varepsilon-\zeta}{kT}}{\left(1+\exp\frac{\varepsilon-\zeta}{kT}\right)^2}$$

is a "pseudo" δ-function centering around the Fermi level, ζ_0. The function $\varepsilon^2f'(\varepsilon)$ in the first term of Eq. (3.16'') has non-zero values in a certain region broader

than the region where the function $f'(\varepsilon)$ in Eq. (3. 11″) has non-zero values, because of the factor of ε^2 in the former. Therefore, the part of the density of states curve which is effective in the integration for γ is broader than that effective for χ_0 at a certain temperature. That is, so far as the temperature dependence of the Fermi level is neglected, the behaviour of γ at a temperature range reflects the behaviour of χ_0 at a certain higher temperature range. Therefore, if there is a maximum or minimum in χ due to the band shape, there will be a steeper maximum or minimum in γ at a temperature lower than the temperature where χ shows the extremum.

§ 4 Determination of Density of States Curves

The density of states curves are determined from specific heat data at very low temperature of some series of transition metals and their alloys on the basis of the rigid band model by means of the HOARE-MATTHEWS-WALLING's method.[9]

In a non-ferromagnetic case, by assuming that the shape of plus-spin sub-band is quite similar to that of minus-spin sub-band and by using the rigid band model, there are following relations between the change in the number of electrons (or holes), n, and the shift of the Fermi level, ε, due to alloying (here the origin of energy is fixed at a certain position in the band) :

$$\varepsilon = \int_0^{n/2} \frac{1}{\nu} d(n/2), \tag{4. 1}$$

where ν is the density of states as a function of $n/2$, which obtained from the value of γ of the corresponding alloy. By graphical integration of $1/\nu$ with respect to $n/2$, ν is determined as a function of ε. In a ferromagnetic case, there are following relations :

$$\left.\begin{aligned} &M/\mu = n_+ - n_-, \\ &n = n_+ + n_-, \\ &\gamma(0) = \gamma_+ + \gamma_- \end{aligned}\right\} \tag{4. 2}$$

and

$$\varepsilon_\pm = \int_0^{n_\pm} \frac{1}{\nu} dn_\pm$$

where M and $\gamma(0)$ are the spontaneous magnetization and the electronic specific heat coefficient at 0°K, respectively. By determining n_+ and n_- from the alloy composition and the observed value of M, and by taking account of the similarity of the shape of the plus-and minus-spin sub-bands, ν is determined as a function of ε.

In Figs. 4~8, the density of states curves obtained in this way for Ti–V–Cr–Fe (3d–b. c. c.), Fe–Ni–Cu (3d–f. c. c.), Zr–Nb–Mo–Tc (4d–b. c. c.), Rh–Pd–Ag (4d–f. c. c.) and Ir–Pt–Au (5d–f. c. c.) systems are shown, respectively.

(*1*) *Ti–V–Cr–Fe system (3d–b. c. c.)*

The density of states curve for Ti–V–Cr–Fe system is shown in Fig. 4, which has been determined from the low temperature specific heat data of b. c. c. Ti–V alloys, V metal, V–Cr alloys, Cr metal, Cr–Fe alloys and Fe metal.[10~12] Fe metal and some Cr–Fe alloys are ferromagnetic and the density of states curve is determined to be consistent with the observed values of the spontaneous magnetization.[13] The values of γ of Ti (h. c. p.),[14] Sc (h. c. p.),[15] Ca (f. c. c.)[16] and K (b. c. c.),[16] in some of which the crystal structure are not b. c. c., have been used to determine the shape of low energy part in the density of states curve.

(*2*) *Fe–Ni–Cu system (3d–f. c. c.)*

The density of states curve for Fe–Ni–Cu system is shown in Fig. 5, which has been determined from the low temperature specific heat data of f. c. c. Fe–Ni alloys, Ni metal, Ni–Cu alloys and Cu metal.[17,18] Fe–Ni alloys, Ni metal and some of Ni–Cu alloys are ferromagnetic and the density of states curve is determined to be consistent with the observed values of the spontaneous magnetization.[13]

(*3*) *Zr–Nb–Mo–Tc system (4d–b. c. c.)*

The density of states curve for Zr–Nb–Mo–Tc system is shown in Fig. 6, which has been determined from the low temperature specific heat data of b. c. c. Zr–Nb alloys, Nb metal, Nb–Mo alloys, Mo metal, Mo–Tc, Mo–Re, Mo–Ru and Mo–Pd alloys.[19] In spite of the fact that in this series Re is not a 4d–element, the values of γ of Mo–Re alloys are used for determination of the density of states curve because the value of γ for $Mo_{0.5}Re_{0.5}$ alloy is close to that of the $Mo_{0.5}Tc_{0.5}$ alloy. Since the value of γ of Re metal seems to be too small and the published value of γ of Tc metal seems to be too large,[20] the values of γ in this range are interpolated from the data on γ of Mo–Re, Mo–Ru and Mo–Pd alloys. The values of γ of Zr (h. c. p.)[20] Y (h. c. p.)[15] and Sr (f. c. c.),[16] in which the crystal structure are not b. c. c., have been used to determine the shape of low energy part in the density of states curve.

(*4*) *Rh–Pd–Ag system (4d–f. c. c.)*

The density of states curve for Rh–Pd–Ag system is shown in Fig. 7, which has been determined from the low temperature specific heat data of f. c. c. Rh metal, Rh–Pd alloys, Pd metal, Pd–Ag alloys and Ag metal.[21,22] The values of γ of Ru (h. c. p.),[23] in which the crystal structure is not f. c. c., has been used to determine the shape of low energy part in the density of states curve.

(5) *Ir–Pt–Au system (5d–f. c. c.)*

The density of states curve for Ir–Pt–Au system is shown in Fig. 8, which has been determined from the low temperature specific heat data of f. c. c. Ir metal, Ir–Pt alloys, Pt metal, Pt–Au alloys and Au metal.[22~24] The values of γ of Os (h. c. p.),[23] in which the crystal structure is not f. c. c., has been used to determine the shape of low energy part in the density of states curve. For comparison, also the density of states curve for Rh–Pd–Ag system is shown by the dashed line.

As shown above, the shapes of the density of states curves determined from the observed values of γ of several series of transition metals and alloys are complicated and quite different from that of free electrons (parabola). Therefore, it is expected that for such a band the temperature dependences of electronic specific heat and magnetic susceptibility will be considerably different from that of free electrons (parabolic band).

§ 5 Calculated Results

Calculations for electronic specific heat and the Pauli paramagnetic susceptibility have been performed by making use of the density of states curves given in § 4 and the formulae given in § 3 by means of the Nagoya University electronic computer. Calculated values of the electronic specific heat coefficients, γ, and the Pauli paramagnetic susceptibility, χ_0, are shown in Figs. 9~20.

(1) *Ti–V–Cr–Fe system (3d–b. c. c.)*

Calculated results of γ and χ_0 for Ti–V–Cr–Fe system are shown in Figs. 9~12. It is easily seen from these figures that the values of γ and χ_0 of an alloy or a metal are not constant. Because of the complexity of the density of states curve, temperature variations of γ and χ_0 are considerably complicated and depending on the position of the Fermi level. It is noticed that the calculated values of γ and χ_0 for V metal decrease with increasing temperature and those for Ti and Cr metals and Cr rich V–Cr alloy increase with increasing temperature. A minimum appears in each of the temperature variation curves of γ and χ_0 for $V_{0.5}Cr_{0.5}$ alloy and a maximum appears in each of those for $V_{0.76}Cr_{0.24}$ alloy. The extrema in γ are sharper and exist at lower temperature than those in corresponding χ_0. It is noticed that the behaviours of temperature variation of γ for these alloy system between 0°K and 600°K resemble closely those of χ_0 between 0°K and 2000°K. This fact supports the argument given in the end of § 3 (4).

(2) *Fe–Ni–Cu system (3d–f. c. c.)*

Calculated results of γ and χ_0 for Fe–Ni–Cu system are shown in Figs. 13 and 14. The values of γ and χ_0 for Ni rich Ni–Cu alloys, for which the Fermi

levels are in the high density part of the density of states curve, decrease with increasing temperature, and the values of γ and χ_0 for Cu rich Ni–Cu alloys, for which the Fermi levels are in the low density part of the density of states curve, increase with increasing temperature. Some Ni–Cu alloys show a maximum in each of the temperature variation curves of γ and χ_0. The maxima in γ are sharper and the temperatures at the maxima are lower than those in χ_0. Although the Fermi level for paramagnetic Ni lies in the high density part of the density of states curve, a flat maximum appears in each of the temperature variation curves of γ and χ_0, since the density of states curve is concave upwards at the Fermi level. The temperatures of maximum in γ and χ_0 for paramagnetic Ni are lower than the Curie temperature of Ni metal.

(3) *Zr–Nb–Mo–Tc system (4d–b. c. c.)*

Calculated results of γ and χ_0 for Zr–Nb–Mo–Tc system are shown in Figs. 15 and 16. Also those for *Zr* metal, which has not b. c. c. structure, by making use of the density of states curve given in Fig. 6 are shown in these figures by the dashed curves. Because of the complexity of the density of states curve, the temperature variations of γ and χ_0 are considerably complicated, depending on the position of the Fermi level. It is noticed that the calculated values of γ and χ_0 for Nb metal decrease with increasing temperature, and those for Mo and Zr metals increase with increasing temperature. The behaviours of temperature variation of γ for these alloy system between 0°K and 600°K resemble closely those for χ_0 between 0°K and 2000°K.

(4) *Rh–Pd–Ag system (4d–f. c. c.)*

Calculated results of γ and χ_0 for Rh–Pd–Ag system are shown in Figs. 17 and 18. For some alloys and Pd metal, Fermi levels of which lie in the neighbourhood of a peak in the density of states curve, the calculated values of γ and χ_0 remarkably decrease with increasing temperature. For these metal and alloys the $\chi_0^{-1}-T$ curves become almost linear at higher temperatures and the Curie-Weiss law holds apparently at higher temperatures. It seems that this is due to the narrow and high peak of the density of states curve at the Fermi levels. That is, such a narrow and high peak of the density of states curve may be approximated as a localized state. Here, the apparent Curie constant will not be determined by localized spin moments as in the case of the localized electron model, but it will be determined by the shape of the density of states curve and the position of the Fermi level.

It is noticed that for $Pd_{0.9}$ $Ag_{0.1}$ alloy a maximum appears in each of the temperature variation curves of γ and χ_0 (minimum in that of χ_0^{-1}), and the maximum in γ is sharper and exist at lower temperature than that of χ_0.

(5) *Ir–Pt–Au system (5d–f. c. c.)*

Calculated results of γ and χ_0 for Ir–Pt–Au system are shown in Figs. 19 and 20. For some alloys and Pt metal, Fermi levels of which lie in the neighbourhood of a peak in the density of states curve, the calculated values of γ and χ_0 decrease remarkably with increasing temperature. For these metal and alloys the $\chi_0^{-1}-T$ curves become alomost linear at higher temperatures and the slopes of these curves are slightly slower for alloys with the lower concentration of Au or higher concentration of Ir. It seems at first sight that the slopes of these curves correspond to the number of holes in the d-band of these alloys. However, since our calculations are based on the band model, it is concluded that a linearity of $\chi^{-1}-T$ curve does not always mean the existence of localized moments and a slope of $\chi^{-1}-T$ curve does not always correspond to a magnitude of magnetic carriers. Several alloys show a minimum in each $\chi_0^{-1}-T$ curve at a certain temperature and a steeper maximum in the corresponding $\gamma-T$ curve at a lower temperature.

§ 6 Electronic Specific Heat

Calculated results of electronic specific heat are compared with the experimental ones estimated in § 2.

(*1*) *"Plus group" metals*

"Plus group" metals for which the calculations of electronic specific heat have been performed are Ti, Cr, Zr, Mo and Rh metals.

a) Cr metal

Cr metal is a typical "plus group" metal. Namely, the estimated values of C_E of Cr metal strikingly larger than $\gamma(0)T$ (Fig. 2C) and the value of γ^* ($\equiv\gamma/\gamma(0)$) are very large above the room temperature (Fig. 3). The calculated values of C_E and γ are compared with the experimental values in Figs. 21 and 22. It is easily seen from these figures that the calculated results well explain the typical character of C_E and γ of Cr metal. This suggests that the density of states curve shown in Fig. 4, where the Fermi level of Cr metal lies at the minimum density of states and a high peak of density of states exists near the Fermi level, is close to the real density of states of Cr metal.

(b Ti metal

The estimated values of C_E of Ti metal are larger than $\gamma(0)T$ below the transition temperature (Fig. 2A) and $\gamma^*>1$ (Fig. 3). The calculated values of C_E and γ are compared with the experimental values in Figs. 23 and 24. Experimental values of C_E are somewhat larger than calculated ones just below the transition temperature and this disagreement may be attributed to the phase transition.

c) Zr metal

The estimated values of C_E of Zr metal are larger than $\gamma(0)T$ (Fig. 2H) and

$\gamma^*>1$ (Fig. 3). Calculated values of C_E and γ are compared with experimental ones in Figs. 25 and 26. As the experimental values in these figures, we have shown not only the ones shown in Fig. 2H but also the one which has been estimated recently by FISHER[25] from the data of SCOTT (unpublished work quoted by FISHER) and also the one which has been estimated from the data given in reference 26. The agreements between the calculated and the experimental results are satisfactory.

d) Mo metal

The estimated values of C_E of Mo metal are larger than $\gamma(0)T$ (Fig. 2J) and $\gamma^*>1$ (Fig. 3). Calculated values of C_E and γ are compared with experimental ones in Figs. 27 and 28. As the experimental values in these figures, we give not only the ones shown in Fig. 2J but also the ones estimated from the data of LOWENTHAL[27] above 1000°K. The agreements between the calculated and the experimental results are satisfactory.

e) Rh metal

The estimated values of C_E of Rh metal are slightly larger than $\gamma(0)T$ (Fig. 2K) and the values of γ^* are almost constant and slightly larger than 1 (Fig. 3). At 2000°K, the estimated value of C_E is slightly smaller than $\gamma(0)T$ and the value of γ^* is slightly smaller than 1. Comparison between calculated and experimental values of C_E and γ are given in Figs. 29 and 26. The calculated results well explain the behaviours of experimental results. It is noticed that the fact $C_E \approx \gamma(0)T$ in Rh metal is not due to the ordinary consequence of the band theory that a parabolic band with a high temperature of degeneracy leads to a constant value of γ, but due to the fact that in Rh metal the Fermi level lies halfway up a slope of the density of states curve and both tendencies of increasing and decreasing γ with increasing temperature are cancelled by each other. It is a rather special case in transition metals that the value of γ are nearly constant such as in Rh metal.

(2) *"Minus group" metals*

"Minus group" metals for which the calculations of electronic specific heat have been performed are V, Ni, Nb, Pd and Pt metals.

a) V metal

The estimated values of C_E of V metal are smaller than $\gamma(0)T$ (Fig. 2B) and $\gamma^*<1$ (Fig. 3). The calculated values of C_E and γ are compared with the experimental ones in Figs. 30 and 31. The agreements of calculated results with experimental results are satisfactory. The experimental values of γ in V metal show a minimum at about 500°K and also the calculated values of γ show a minimum at somewhat different temperature.

b) Ni metal

Although Ni metal is ferromagnetic, the estimated values of C_E above the Curie temperature are smaller than $\gamma(0)T$ (Fig. 2G) and $\gamma^*<1$ (Fig. 1C). Comparisons between calculated and experimental values of C_E and γ for paramagnetic Ni metal (above the Curie temperature) are given in Figs. 32 and 33. The agreements between the calculated and the experimental results are satisfactory.

c) Nb metal

The estimated values of C_E of Nb metal are smaller than $\gamma(0)T$ (Fig. 2I) and $\gamma^*<1$ (Fig. 3). Comparisons between calculated and experimental values are given in Figs. 34 and 35. As the experimental values in these figures, we give not only the ones shown in Fig. 2I but also the ones estimated from the data of LOWENTHAL[27] above 1000°K. The agreements between the calculated and the experimental results are satisfactory.

d) Pd metal

The estimated values of C_E of Pd metal are smaller than $\gamma(0)T$ (Fig. 2L) and $\gamma^*<1$ (Fig. 3). The calculated values of C_E and γ are compared with experimental ones in Figs. 36 and 37. The agreements between the calculated and the experimental results are satisfactory.

e) Pt metal

The estimated values of C_E of Pt metal are smaller than $\gamma(0)T$ (Fig. 2Q) and $\gamma^*<1$ (Fig. 3). The calculated values of C_E and γ are compared with experimental ones in Figs. 38 and 39. The agreements between calculated and the experimental results are satisfactory.

As we have shown above, the calculated results of C_E by making use of the density of states curves determined from the low temperature specific heat data of several series of transition metals and alloys on the basis of the rigid band model well explain the characteristic behaviours of the temperature variation of electronic specific heat of the transition metals. This fact seems to suggest that the density of states curves determined in § 4 are fairly close to the real ones of transition metals. Therefore, it will be significant to calculate the Pauli paramagnetic susceptibility over a wide range of temperatures by making use of the density of states curves, to compare the calculated results with the experimental values of magnetic susceptibility and to estimate the values of the orbital paramagnetic susceptibility and the molecular field coefficient for the transition metals and their alloys.

§ 7 Magnetic Susceptibility

The values of the Pauli paramagnetic susceptibility, χ_0, calculated in § 5 are considerably smaller than observed values of χ. The differnce between calculated χ_0 and observed χ will be attributed to the effects of molecular field, orbital

paramagnetism and core- and orbital(Landau)-diamagnetism.

Following relations are assumed between χ_0 and χ :

$$\left.\begin{aligned} &\chi = \chi_{spin} + \chi_c, \\ &\chi_{spin}^{-1} = \chi_0^{-1} - \alpha, \\ &\text{and} \\ &\chi_c = \chi_{orb.} + \chi_{dia.}, \end{aligned}\right\} \quad (7.1)$$

where α, $\chi_{orb.}$ and $\chi_{dia.}$ are the molecular field coefficient, the orbital paramagnetic susceptibility and the sum of core- and orbital-diamagnetic susceptibility, respectively. Since the effective mass of electrons in transition metals is generaly large, the contribution of the orbital diamagnetism will be neglected.

It is expected that the density of states curves determined in § 4 are very close to the real ones, as shown in the discussions on electronic specific heat. Therefore, it will be significant to estimate the values of α and $\chi_{orb.}$ for transition metals and their alloys by comparing the values of χ_0 calculated for these density of states curves with observed values of χ over a wide range of temperatures. In these comparisons, we have neglected the temperature variations of α, $\chi_{orb.}$ and $\chi_{dia.}$ for the sake of simplicity as these temperature variations are expected to be small.

(*1*) *Ti–V–Cr–Fe system* (*3d–b. c. c.*)

a) V–Cr alloys

Temperature variations of χ of V–Cr alloys are depending on the composition, that is, the values of χ decrease with increasing temperature in V metal[28,29] and in V rich V–Cr alloys,[30] and increase with increasing temperature in Cr rich V–Cr alloys[30] and in Cr metal.[29~31] In $V_{0.5}$ $Cr_{0.5}$ alloy, a minimum appears in the temperature variations of χ.[30] Calculated results of χ_0 show such a tendency (Fig. 11), although the calculated values of χ_0 are considerably smaller than the observed values of χ. These disagreements are attributed to the temperature independent orbital paramagnetic susceptibilities, $\chi_{orb.}$. Assuming the relation,

$$\chi = \chi_0 + \chi_{orb.},$$

and taking the values of $\chi_{orb.}$ shown in Table 2, we obtain an excellent agreements between calculated and experimental results as shown in Figs. 40 and 41. This fact shows that the molecular field is negligible in V–Cr alloys. Here, we have neglected the effects of core- and orbital-diamagnetism. Composition dependence of $\chi_{orb.}$ estimated for V–Cr alloys is shown in Fig. 42. The values of $\chi_{orb.}$ and their composition dependence given in Table 2 and Fig. 42 seem to be reasonable.

Table 2 Orbital paramagnetic susceptibilities, $\chi_{orb.}$, for V and Cr metals and V–Cr alloys.

Composition	$\chi_{orb.}$ (10^{-4} emu/mole)
V	1.78
$V_{0.75}$ $Cr_{0.25}$	1.70
$V_{0.5}$ $Cr_{0.5}$	1.70
$V_{0.25}$ $Cr_{0.75}$	1.45
Cr	1.35

b) V–Ti alloys

Also the calculated results of χ_0 in V–Ti alloys (Fig. 9) explain qualitatively the experimental results that the values of χ increase with increasing temperature in Ti metal[28,32] and decrease with increasing temperature in V metal and V rich V– Ti alloys.[30] Assuming the relation,

$$\chi = (\chi_0^{-1} - \alpha)^{-1} + \chi_{orb.},$$

and taking the values of α and $\chi_{orb.}$ shown in Table 3, we obtain an agreement between calculated and experimental results except for $V_{0.25}Ti_{0.75}$ alloy at low temperatures (this disagreement is due to the phase transition of this alloy), as shown in Figs. 43 and 44. Here, we have neglected $\chi_{dia.}$. The values of α and $\chi_{orb.}$ given in Table 3 are not always reliable. Probably, at least, the absolute values of α in $V_{0.5}$ $Ti_{0.5}$ alloy and in Ti metal will be smaller, and the value of $\chi_{orb.}$ in $V_{0.5}$ $Ti_{0.5}$ alloy will be larger and that in Ti metal will be smaller than the value given in the table.

Table 3 Molecular field coefficients, α, and orbital paramagnetic susceptibilities, $\chi_{orb.}$, for V and Ti metals and V–Ti alloys.

Composition	α(10^4 mole/emu)	$\chi_{orb.}$ (10^{-4} emu/mole)
V	0.00	1.78
$V_{0.75}$ $Ti_{0.25}$	−0.32	1.85
$V_{0.5}$ $Ti_{0.5}$	−0.80	2.00
$V_{0.25}$ $Ti_{0.75}$	−0.10	1.70
Ti	+0.82	0.73

c) Cr–Fe and Cr–Mn alloys

The values of χ in Cr–Fe alloys are considerably larger than those in Cr–Mn alloys with common value of electron per atom ratio, e/a. For example, the

value of χ at room temperature in $Cr_{0.95}$ $Fe_{0.05}$ alloy[33,34] is about 1.8 times as large as that in $Cr_{0.9}$ $Mn_{0.1}$ alloy,[30] that in $Cr_{0.9}$ $Fe_{0.1}$ alloy[34] is about 2.6 times as large as that in $Cr_{0.8}$ $Mn_{0.2}$ alloy[30] and that in $Cr_{0.85}$ $Fe_{0.15}$ alloy[33,34] is about 5.3 times as large as that in $Cr_{0.7}$ $Mn_{0.3}$ alloy.[30] This fact seems to mean that the effect of molecular field is the main mechanism of enhancement in Cr–Fe alloys, while the molecular field is not so effective in Cr–Mn alloys.

For Cr rich Cr–Mn alloys ($e/a \leqq 6.2$, where $e/a=6$ for Cr metal), assuming the relation,

$$\chi = \chi_0 + \chi_c,$$

and taking the values of χ_c shown in Table 4, we obtain good agreements between calculated and experimental values as shown in Fig. 45. The experimental

Table 4 Molecular field coefficients, α, temerature independent susceptibilities, χ_c, and enhancements of spin paramagnetic susceptibilities, $\chi_{spin}-\chi_0$, for Cr metal and Cr–Mn alloys.

Composition	$\alpha(10^4$ mole/emu)	$\chi_c(10^{-4}$ emu/mole)	$\chi_{spin}-\chi_0(10^{-4}$ emu/mole)	
			300°K	1000°K
Cr	0	1.35	0	0
$Cr_{0.9}$ $Mn_{0.1}$	0	1.50	0	0
$Cr_{0.8}$ $Mn_{0.2}$	0	1.76	0	0
$Cr_{0.7}$ $Mn_{0.3}$	0.171	1.62	0.6	0.2
$Cr_{0.6}$ $Mn_{0.4}$	0.148	1.66	0.8	0.2
$Cr_{0.5}$ $Mn_{0.5}$	0.211	1.95	1.8	0.4

values of χ in $Cr_{0.9}$ $Mn_{0.1}$ alloy increase with increasing temperature above room temperature.[30] The calculated values of χ for Mn 4.25 atomic % alloy show a minimum at 100°K and increase with increasing temperature above 100°K, and those for Mn 6.4 atomic % alloy show a minimum at 400°K and increase with increasing temperature above 400°K. If an uncertainty of the density of states is taken into account, it may be concluded that the increase of χ with increasing temperature in $Cr_{0.9}$ $Mn_{0.1}$ alloy is due to the shape of the density of states curve and the position of the Fermi level. The agreements between calculated and experimental results are fairly good.

For Mn rich Cr–Mn alloys ($e/a \geqq 6.3$), the effect of the molecular field must be taken into account. By using the Eqs. (7.1) and by adjusting the values of α and χ_c to make agree the values of calculated χ with experimental ones at 300°K

and 1200°K, we obtain the values of α and χ_c shown in Table 4. The calculated results by making use of these values of α and χ_c are compared with the experimental results[30] in Fig. 46. Agreements between calculated and experimental results are good. In Cr–Mn alloys the values of χ_c are larger than that in Cr metal as shown in Table 4. This will be due to the fact that as the density of states at the Fermi levels of these alloys is very larger than that of Cr metal as shown in Fig. 4, many states with small energy difference will be combined by the orbital angular momentum and $\chi_{orb.}$ will be large. In these alloys the main mechanism of enhancement of χ is the orbital paramagnetism. As shown in Table 4, the calculated values of $\chi_{spin} - \chi_0$ at 300°K and 1000°K are considerably smaller than the values of χ_c.

In Cr–Fe alloys, the effect of molecular field is predominant. Assuming the relation,

$$\chi^{-1} = \chi_0^{-1} - \alpha,$$

and taking the values of $\alpha = 1.0 \times 10^4$mole/emu for $Cr_{0.95}Fe_{0.05}$ alloy, $\alpha = 0.66 \times 10^4$mole/emu for $Cr_{0.9}Fe_{0.1}$ alloy, and $\alpha = 0.54 \times 10^4$mole/emu for $Cr_{0.85}Fe_{0.15}$ alloy, the calculated values of χ^{-1} roughly agree with experimental values[33,34] as shown in Fig. 47.

Table 5 Molecular field coefficients, α, for Cr–Fe alloys.

Composition	$\alpha(10^4$ mole/emu)
$Cr_{0.95}Fe_{0.05}$	1.00
$Cr_{0.9}Fe_{0.1}$	0.66
$Cr_{0.85}Fe_{0.15}$	0.54

d) Fe metal

Calculated values of χ_0 for paramagnetic Fe metal by using the density of states curve given in Fig. 4 increase with increasing temperature as shown by curve (1) in Fig. 48 (b), whereas the observed values of χ for b. c. c. Fe metal decrease with increasing temperature above the Curie temperature.[35] Curve (1′) in the figure is the value of $\chi_{obs.}^{-1} + 1.183 \times 10^4$mole/emu for b. c. c. Fe metal.

We have determined a new density of states curve for Fe metal.[36] This has been deduced from the experimental data of γ,[10,11] and of spontaneous magnetization for b. c. c. 3d-group transition metals and their alloys[37,38] and assuming the rigid band model. Here, only those specific heat measurements were used for which C/T–T^2 curves were accurately linear and gave reasonable value for

the Debye temperature (accordingly the data of γ for Cr–Fe alloys of lower concentrations than 30 atomic % Fe were neglected); the data of spontaneous magnetization used in this analysis were corrected for g–factor using the data and relation (6) of reference 39. The new density of states curve, as shown by a thick curve (2) in Fig. 49, differs from the old one given in Fig. 4 (shown by a thin curve (1) in Fig. 49) particularly in not having such a pronounced peak at an electron per atom ratio, e/a, near 6.4.

The calculated values of χ_0 for paramagnetic Fe metal by using the new density of states curve show a maximum at about 1100°K and decrease with increasing temperature above the temperature as shown by curve (2) in Fig. 48 (b) (the Curie temperature of Fe metal is about 1040°K). Curve (2′) in the figure is the values of $\chi_{obs.}^{-1} + 0.963 \times 10^4$ mole/emu for b.c.c. Fe metal. The agreement with observation of χ of calculated χ corrected by taking account of a molecular field by using the new density of states curve is much better than that obtained by using the old one.

The calculated results of C_E obtained by using the old density of states curve and by using the new one are shown by curves (1) and (2) in Fig. 48 (a), respectively. Small circles in the figure are experimental values of C_E in δ–phase Fe estimated by the method given in § 2, and curve (3) was obtained from the smoothed and extrapolated curve of experimental C_p.[40] It seems that the agreement with observation of calculated C_E by using the new density of states curve is a little better than that obtained by using the old one.

Therefore, it will be concluded that, at least, for Fe metal the new density of states curve is more adequate than the old one.

(2) *Ni–Cu system (3d–f. c. c.)*

Calculated values of χ_0 for Ni metal and Ni–Cu alloys with high concentration of Ni ($\gtrsim$40 atomic %) decrease with increasing temperature above room temperature and those for Ni–Cu alloys with low concentration of Ni ($\lesssim$20 atomic %) increasing with increasing temperature. This results qualitatively agree with experimental ones.[35,41~45]

a) Ni metal and Ni rich Ni–Cu alloys

Assuming the relation,

$$\chi_0(T_c)^{-1} - \alpha = 0,$$

for Ni metal and Ni rich ferromagnetic Ni–Cu alloys, we obtain the values of α as follow :

$\alpha = 0.96 \times 10^4$ mole/emu for Ni metal,

$\alpha = 0.99 \times 10^4$ mole/emu for $Ni_{0.75}$ $Cu_{0.25}$ alloy

and

$\alpha = 1.03 \times 10^4$ mole/emu for $Ni_{0.5}$ $Cu_{0.5}$ alloy.
The value of χ^{-1} calculated by the relation,

$$\chi^{-1} = \chi_0^{-1} - \alpha,$$

and by making use of the values of α estimated above are compared with the observed values[35, 41, 42, 45] in Figs. 50, 51 and 52, respectively, for Ni metal, $Ni_{0.75}$ $Cu_{0.25}$ and $Ni_{0.5}$ $Cu_{0.5}$ alloys. Calculated values of χ^{-1} are smaller than the observed ones above Curie temperatures, and calculated results do not explain the fact that the observed $\chi^{-1}-T$ curves are concave downwards. Taking account of the effect of constant paramagnetic susceptibility, χ_c, by Eqs. (7.1), we obtain better agreements at high temperatures, Taking the values of $\alpha = 0.880 \times 10^4$mole/emu and $\chi_c = 0.71 \times 10^{-4}$ emu/mole for Ni metal, we obtain the curve (2) in Fig. 50. However, in this case, $\chi^{-1} > 0$ at the Curie temperature. Even though we take into account a temperature variation of $\chi_{orb.}$ due to the temperature dependence of χ_{spin} via spin-orbit interaction, the situation is not improved (curve (3) in Fig. 50). Taking the values of $\alpha = 0.829 \times 10^4$ mole/emu and $\chi_c = 0.4 \times 10^{-4}$ emu/mole for $Ni_{0.75}$ $Cu_{0.25}$ alloy, we obtain the curve (2) in Fig. 51, and taking the values of $\alpha = 0.762 \times 10^4$ mole/emu and $\chi_c = 0.6 \times 10^{-4}$ emu/mole, we obtain the curve (3). The agreements with experiments become better at high temperatures, but $\chi^{-1} > 0$ at the Curie temperature. Taking the values of $\alpha = 0.678 \times 10^4$ mole/emu and $\chi_c = 0.4 \times 10^{-4}$ emu/mole for $Ni_{0.5}$ $Cu_{0.5}$ alloy, we obtain the curve (2) in Fig. 52, and taking the values of $\alpha = 0.622 \times 10^4$ mole/emu and $\chi_c = 0.5 \times 10^{-4}$ emu/mole, we obtain the curve (3). The agreements with experiments become better at high temperatures, but $\chi^{-1} > 0$ at the Curie temrepature.

To obtain good agreements between calculated and observed values of χ^{-1} above Curie temperatures for Ni metal and ferromagnetic Ni-Cu alloys, it seems to be necessary to take account of the temperature variations of α and χ_c. Otherwise, the disagreements between calculated and observed results may be attributed to an uncertainty of the density of states curve.

b) Cu rich Ni-Cu alloys

The values of χ calculated by Eqs. (7.1) from the calculated values of χ_0 for Cu rich (paramagnetic) Ni-Cu alloys are compared with observed values[43~45] in Figs. 53, 54 and 55. Here, we take the values of $\alpha = 0.556 \times 10^4$ mole/emu and $\chi_c = 0.20 \times 10^{-4}$ emu/mole for $Ni_{0.4}$ $Cu_{0.6}$ alloy (Fig. 53), $\alpha = 0.393 \times 10^4$ mole/emu and $\chi_c = 0.07 \times 10^{-4}$ emu/mole for $Ni_{0.2}$ $Cu_{0.8}$ alloy (Fig. 54), and $\alpha = 0.278 \times 10^4$ mole/emu and $\chi_c = -0.056 \times 10^{-4}$ emu/mole for $Ni_{0.1}$ $Cu_{0.9}$ alloy (Fig. 55).

Composition dependences of α and χ_c estimated above are shown in Fig. 56.

(3) *Zr-Nb-Mo-Tc system (4d-b. c. c.)*

a) Nb-Mo alloys

Calculated results of χ_0 qualitatively explain the fact that the observed values of χ decrease with increasing temperature in Nb metal and Nb rich Nb–Mo alloys, and increase with increasing temperature in Mo metal and Mo rich Nb–Mo alloys.[20] However, the calculated values of χ_0 are considerably smaller than observed values of χ. Assuming the relation,

$$\chi = \chi_0 + \chi_c,$$

for Mo metal and Mo rich Nb–Mo alloys, and taking the values of $\chi_c = 0.544 \times 10^{-4}$, 0.521×10^{-4} and 1.221×10^{-4} emu/mole for Mo metal, $Mo_{0.75}$ $Nb_{0.25}$ and $Mo_{0.5}$ $Nb_{0.5}$ alloys, respectively, we obtain agreements between calculated and experimental values[30] as shown in Fig. 57. This means that $\chi_{spin} = \chi_0$ or $\alpha = 0$ in Mo metal and Mo rich Nb–Mo alloys. For Nb metal and Nb rich Nb–Mo alloys, we obtain agreements between calculated and experimental values[30] by Eqs. (7. 1) taking the values of $\alpha = -0.204 \times 10^4$ mole/emu and $\chi_c = 0.98 \times 10^{-4}$ emu/mole for Nb metal, and $\alpha = 0.260 \times 10^4$ mole/emu and $\chi_c = 0.94 \times 10^{-4}$ emu/mole for $Nb_{0.75}$ $Mo_{0.25}$ alloy as shown in Fig. 58.

Several measurements on χ have been made for Nb–Mo,[30,46~48] Nb–Re[46] and Nb–Tc[49] alloys. These observed values of χ at room temperature plotted to the value of e/a are somewhat different from each other. We estimate the value of χ_c as $\chi_c = 0.60 \times 10^{-4}$ emu/mole for Mo metal from a comparison of calculated value of χ_0 at 300°K ($\chi_0(300°K) = 0.28 \times 10^{-4}$ emu/mole) with the mean value of observed χ at room temperature (0.88×10^{-4} emu/mole). Using the values of χ_c for Mo and Nb metals and $Nb_{0.75}$ $Mo_{0.25}$ alloy estimated above and assuming the composition dependence of $\chi_{orb.}$ similar to that for V–Cr alloys, we obtain the composition dependence of χ_c in Nb–Mo alloys. This is shown by the smooth curve in Fig. 59. If we neglect $\chi_{dia.}$, χ_c will be regarded as $\chi_{orb.}$. These values of $\chi_{orb.}$ are shown in second column of Table 9. If the value of $\chi_{dia.}$ in these metals and alloys is similar to that in Pd metal, the values of $\chi_{orb.}$ are larger than that given in Fig. 59 and in Table 9 by 0.21×10^{-4} emu/mole.[50]

The value of χ_{spin} for each composition is estimated in the following way : in the Mo rich alloys ($e/a \geqq 5.5$) $\chi_{spin} = \chi_0$, in the Nb rich alloys ($e/a \leqq 5.25$) $\chi_{spin} = (\chi_0^{-1} - \alpha)^{-1}$, and in the intermediate range the values of χ_{spin} are obtained by joining smoothly as shown in Fig. 60. Thus the value of χ_{spin} is determined for each composition in the Nb–Mo alloys (Fig. 60). Values of the sum of χ_c and χ_{spin} are shown in Fig. 61. These values roughly agree with observed values of χ.

b) Zr metal

Although the crystal structure of Zr metal is not b. c. c., we calculate χ_0 by making use of the density of states curve given in Fig. 6. The value of the

density of states at the Fermi level of Zr in Fig. 6 has been determined from the value of γ in h. c. p. Zr metal. The experimental data of χ in Zr metal[30,32] are somewhat different from each other as shown in Fig. 62. Calculated values of χ_0 are considerably smaller than the observed ones. Assuming the relation,

$$\chi = \chi_0 + \chi_c,$$

and taking the value of $\chi_c = 0.8 \times 10^{-4}$ emu/mole, the calculated values of χ lie between the two observed data as shown by curve (1) in Fig. 62. The value of $\chi_c = 0.8 \times 10^{-4}$ emu/mole for Zr metal is somewhat smaller than that for Nb metal (0.98×10^{-4} emu/mole) and this is reasonable. Assuming the relation (7. 1) and taking the values of $\alpha = -1.37 \times 10^4$ mole/emu and $\chi_c = 0.95 \times 10^{-4}$ emu/mole, we obtain calculated values of χ (curve (2) in Fig. 62) which fairly agree with the data of TANIGUCHI, TEBBLE and WILLIAMS[30] between 300°K and 800°K. Above 800°K, the observed values rapidly increase with increasing temperature and disagree with the calculated values. This behaviour will be attributable to the phase transition occuring at about 1200°K.[30] By taking the values of $\alpha = 0.37 \times 10^4$ mole/emu and $\chi_c = 0.71 \times 10^{-4}$ emu/mole, the calculated values agree with the data of SQUIRE and KAUFMANN[32] between 300°K and 1000°K (curve (3) in Fig. 62). The calculated result is very flat compared with the data of SK below room temperature. An extrapolation of the data of TTW seems to be flat below room temperature.

It will be concluded from the analysis given above that the value of χ_c of Zr metal is between 0.95×10^{-4} and 0.71×10^{-4} emu/mole, that is, about 0.8×10^{-4} emu/mole. Assuming the same value of $\chi_{dia.} = -0.21 \times 10^{-4}$ emu/mole for Pd metal,[50] the value of $\chi_{orb.}$ for Zr metal is given as $\chi_{orb.} = 1.0 \times 10^{-4}$ emu/mole. On the value of α we cannot draw any definite conclusion.

(4) *Rh–Pd–Ag system (4d–f. c. c.)*

a) Pd metal

The calculated values of χ_0 are considerably smaller than observed values of χ[28,50,51] (Fig. 63). This disagreement is mainly attributed to the effect of a molecular field. Assuming the relation,

$$\chi^{-1} = \chi_0^{-1} - \alpha,$$

and taking the value of $\alpha = 0.724 \times 10^4$ mole/emu, we obtain a good agreement of calculated result with experimental ones above room temperature as shown in Fig. 64. Since $\chi_{dia.} = -0.21 \times 10^{-4}$ emu/mole in Pd metal,[50] the value of $\chi_{orb.}$ is estimated as $\chi_{orb.} = 0.21 \times 10^{-4}$ emu/mole. This value of $\chi_{orb.}$ is considerably smaller than that for V, Cr and Nb metals. This is reasonable, because it is expected that the Fermi levels of V, Cr and Nb metals lie in the middle of the

d-band and there are so many states which can be combined by the orbital angular momentum that the values of $\chi_{orb.}$ in these metals are relatively large, while the Fermi level of Pd metal lies in the vicinity of the upper end of the 4d-band and the value of $\chi_{orb.}$ is relatively small.

Below the room temperature, the observed χ shows a maximum at about 80°K,[50] whereas the calculated result of χ_0 for the density of states curve given in Fig. 7 does not show such a maximum. Following the RHODES' idea[52] that the density of states curve has a small dent at the Fermi level, the calculated result shows a maximum. Such an example is shown in Fig. 65. That is, the density of states is slightly modified to have a small hump at the position higher than the Fermi level of Pd by 100(°K)k where k is Boltzmann's constant. Such a slight modification yields little change in the calculated values of χ_0 (and C_E) at high temperatures. The position of the small hump in the density of states given in Fig. 65 corresponds to the Fermi level of $Pd_{0.97}$ $Ag_{0.03}$ alloy. The calculated result of χ_0 for this density of states curve shows a maximum at about 50°K. Therefore, to obtain a maximum at 80°K, the position of the small hump in the density of states curve must be higher than the previous position, that is, it will correspond to the Fermi level of an alloy with 5 or 6 atomic % of Ag. If it was so, the values of $\gamma(0)$ for Pd-Ag alloys must increase with increasing Ag concentration up to about 5 or 6 atomic %. But observed values of $\gamma(0)$ decrease monotonically with Ag concentration.[22] If the curvature of the density of states curve at the Fermi level is larger than that in Fig. 7 and the position of the Fermi level of Pd is farther from the position of the peak of the density of states than that in Fig. 7, there is a possibility that the calculated values of χ_0 show a maximum at 80°K without such a dent in the density of states curve as suggested by RHODES. This argument is supported by the fact that the calculated values of χ_0 for $Pd_{0.9}$ $Ag_{0.1}$ alloy, the Fermi level of which is higher than that of Pd metal by about 0.028 eV, show a maximum at about 120°K as shown in Fig. 18. We have discussed in § 3 (4) on the general possibility that in certain case χ_0 shows a maximum.

It is possible, in principle, to decide which type of mechanism, antiferromagnetism or the special band shape, is responsible for the maximum in the observed χ in following way :

1. neutron diffraction
   Below 80°K, is the antiferromagnetic structure observed, or not ?
2. specific heat
   At about 80°K, is the anomaly of the specific heat corresponding to the antiferromagnetic transition observed, or not ?

Hitherto, there is no evidence to show that the maximum at about 80°K in

observed χ is due to antiferromagnetism. That is, no antiferromagnetic structure has been reported from neutron diffraction data, and no anomaly of the specific heat at corresponding temperature has been observed.[53]

As we have discussed in § 3 (4), at a certain temperature the width of the part of the band responsible for C_E is broader than that responsible for χ, and it is expected that the behaviour of γ at a temperature range reflects the behaviour of χ at a certain higher temperature range. In fact, for $Pd_{0.9}Ag_{0.1}$ alloy, the calculated values of χ_0 show a maximum at about 120°K and $(\chi_0^{max} - \chi_0(0))/\chi_0(0) = 0.94\%$, while the calculated values of γ show a maximum at about 80°K and $(\gamma^{max} - \gamma(0))/\gamma(0) = 2.0\%$ (Fig. 66). Therefore, if the maximum at about 80°K in χ of Pd metal is due to the band shape, it will be expected that a maximum in γ also appears at about 40°K to 60°K. In this case, observed values of γ will show a temperature variation as shown schematically in Fig. 67. It is, however, doubtful that this maximum is observed experimentally or not. From the measurements[50] $(\chi^{max} - \chi(0))/\chi(0) = 3.3\%$. If there is a maximum in γ, it is expected that $(\gamma^{max} - \gamma(0))/\gamma(0) \approx 3 \sim 7\%$. From this value, the anomaly in the electronic specific heat ΔC_E is estimated as $\Delta C_E/C_E \approx 3 \sim 7\%$. As $C_E \approx 0.1\ C_D$ in this temperature range, $\Delta C_E/C_p \approx 0.3 \sim 0.7\%$. This is too small to be detected at present.

b) Pd–Ag and Pd–Rh alloys

Taking into consideration the effects of the molecular field, the orbital paramagnetism and the core- and orbital-diamagnetism by Eqs. (7.1) from the calculated values of χ_0, we calculate the values of χ for Pd–Ag and Pd–Rh alloys with low concentration of Ag and Rh. Here, we take the values of α and χ_c shown in Table 6 for each alloy. Calculated results of χ roughly agree with experimental ones[9,22,51,54] as shown in Figs. 68~71. The values of α and χ_c of these alloys given in Table 6 seem to be reasonable comparing with those of Pd metal,

Table 6 Molecular field coefficients, α, temperature independent susceptibilities, χ_c, and orbital paramagnetic susceptibilities, $\chi_{orb.}$ for Pd metal and Pd–Ag and Pd–Rh alloys.

Composition	α(10^4 mole/emu)	χ_c(10^{-4} emu/mole)	$\chi_{orb.}$(10^{-4} emu/mole)
Pd	0.724	0	0.21
$Pd_{0.969}$ $Ag_{0.031}$	0.72	0	0.21
$Pd_{0.927}$ $Ag_{0.073}$	0.716	−0.072	0.14
$Pd_{0.901}$ $Ag_{0.099}$	0.716	−0.072	0.14
$Pd_{0.861}$ $Ag_{0.139}$	0.76	−0.22	−0.01
$Pd_{0.740}$ $Ag_{0.260}$	0.72	−0.23	−0.02
$Pd_{0.934}$ $Rh_{0.066}$	0.72	0	0.21
$Pd_{0.901}$ $Rh_{0.099}$	0.70	+0.39	0.60

except for the too large value of $\chi_{orb.}$ of the alloy with 9.9 atomic % of Rh. The values of $\chi_{orb.}$ in this table are obtained from the values of χ_c by the relation, $\chi_{orb.} = \chi_c - \chi_{dia.}$ where $\chi_{dia.}$ is assumed to have same value as that of Pd metal, -0.21×10^{-4} emu/mole.[50] Negative value of $\chi_{orb.}$ means that the Landau diamagnetism exceeds orbital paramagnetism.

c) Rh metal

The experimental values of χ of Rh metal rapidly increase with increasing temperature and show a maximum at about 1600°K[28,50] (curves specified by HM and by KTW in Fig. 72) The calculated χ_0 is almost constant and shows a very flat maximum at about 1200°K (curve (1) in Fig 72). If we determine the values of α and χ_c by making the calculated χ given by Eqs. (7.1) equal to the observed values at 0°K and at the maximum point, we obtain the values of $\alpha = 1.33 \times 10^4$ mole/emu and $\chi_c = -3.22 \times 10^{-4}$ emu/mole (curve (2) in Fig. 72). If we take the value of $\alpha = 0.7 \times 10^4$ mole/emu which is similar to that of Pd metal, the values of χ_{spin} are obtained as shown by curve (3) in the figure. Although the maximum in the curve (3) is more remarkable than that in χ_0, curve (1), the experimental curve is steeper than the curve (3). It may be able to make the χ_{spin} curve steeper by a modification of the density of states curve, but in this case the calculated C_E will show a more rapid increase with increasing temperature and the agreement between calculated and experimental C_E obtained in § 6 will be broken.

The temperature variation of observed χ may be due to any effect other than the spin paramagnetism, that is, probably due to the temperature variation of the orbital paramagnetism or the Landau diamagnetism. From this point of view, it is of interest to investigate the temperature variation of the NMR shift, K, in Rh metal in relation to the temperature variation of χ. If the temperature variation of χ is due to the temperature variation of χ_{spin}, the value of K will decrease with increasing χ or with increasing temperature, while if the temperature variation of χ is due to the temperature variation of $\chi_{orb.}$, the value of K will increase with increasing χ or with increasing temperature (cf. § 8).

(5) *Ir–Pt–Au system (5d–f. c. c.)*

a) Pt metal

Calculated values of χ_0 for Pt metal are considerably smaller than observed values of χ.[22,28,50] Assuming the relation (7.1) and taking thev alues of $\alpha = 0.74 \times 10^4$ mole/emu and $\chi_c = -0.15 \times 10^{-4}$ emu/mole, we obtain a good agreement between calculated and experimental results at high temperatures as shown by curve (1) in Fig. 73, whereas this agreement does not hold below room temperature. Since the values of $\chi_{dia.}$ is estimated as $\chi_{dia.} = -0.275 \times 10^{-4}$ emu/mole,[50] the value of $\chi_{orb.}$ is estimated as $\chi_{orb.} = 0.125 \times 10^{-4}$ emu/mole from the value of χ_c given

above. Below room temperature, taking the values of $\alpha = 0.64 \times 10^4$ mole/emu and $\chi_c = 0.2 \times 10^{-4}$ emu/mole, that is, $\chi_{orb.} = 0.475 \times 10^{-4}$ emu/mole, we obtain a good agreement of calculated result with experimental result between 200°K and 300°K. In this case, the calculated values are larger than observed ones at high and low temperatures (curve (2) in Fig. 73).

The values of α and χ_c estimated above are consistent with the values of α and χ_c estimated from the relation between χ and NMR shift in Pt metal.[55] The values of $\chi_{orb.}$ estimated for Pt metal are considerably smaller than those of V, Cr and Nb metals. This will be due to the same situation as that in the case of Pd metal discussed in § 7 (4) a).

The values of α estimated for Pt metal are similar to that estimated for Pd metal. For Pt metal the value of $\chi_0(0)^{-1} = 1.120 \times 10^4$ mole/emu is much larger than the value of α, $0.64 \sim 0.74 \times 10^4$ mole/emu, whereas for Pd metal the value of $\chi_0(0)^{-1} = 0.783 \times 10^4$ mole/emu is slightly larger than the value of α, 0.724×10^4 mole/emu. The fact that very dilute alloys of Co and Fe in Pd and Pt are ferromagnetic and the Curie temperatures are higher in the Pd alloys than that in the Pt alloys, and the fact that very dilute alloys of Ni in Pd and Pt are not ferromagnetic[56] suggest that the electronic state of the impurity (localized or itinerant) will closely connected with the magnetic property of the very dilute alloy (ferromagnetic or not) and the relation between values of α and $\chi_0(0)^{-1}$ will be important to determine the Curie temperature of ferromagnetic very dilute alloy.

b) Pt–Ir and Pt–Au alloys

Taking into consideration the effects of the molecular field, the orbital paramagnetism and the core- and orbital-diamagnetism by Eqs. (7.1) from the calculated values of χ_0, we calculate the values of χ for Pt–Au and Pt–Ir alloys with low concentration of Au and Ir. Here, we take the values of α and χ_c shown in

Table 7 Molecular field coefficients, α, temperature independent susceptibilities, χ_c, and orbital paramagnetic susceptibilities, $\chi_{orb.}$ for Pt metal and Pt–Au and Pt–Ir alloys.

Composition	α (10^4 mole/emu)	χ_c (10^{-4} emu/mole)	$\chi_{orb.}$ (10^{-4} emu/mole)
Pt (high temp.)	0.74	−0.15	0.125
Pt (low temp.)	0.64	0.2	0.475
$Pt_{0.957}$ $Au_{0.043}$	0.63	0.01	0.285
$Pt_{0.899}$ $Au_{0.101}$	0.62	0.01	0.285
$Pt_{0.944}$ $Ir_{0.056}$	0.59	0.19	0.465
$Pt_{0.900}$ $Ir_{0.100}$	0.60	0.04	0.315

Table 7 for each alloy. Calculated results agree with experimental ones[22] between 200°K and 300°K as shown in Fig. 74. The values of $\chi_{orb.}$ in Table 7 are obtained from the value of χ_c by the relation, $\chi_{orb.} = \chi_c - \chi_{dia.}$ where $\chi_{dia.}$ is assumed to have same value as that of Pt metal, -0.275×10^{-4} emu/mole.

§ 8 NMR Shift

In § 7, we have estimated the values of the orbital paramagnetic susceptibility, $\chi_{orb.}$, and the molecular field coefficient, α, for several transition metals and their alloys from the comparison between the calculated values of the Pauli paramagnetic susceptibility, χ_0, and the observed values of magnetic susceptibility, χ, over a wide range of temperatures. In this section, we attempt to explain the NMR shift of V^{51} in V–Cr alloys and Nb^{93} and Tc^{99} in Nb–Mo and Nb–Tc alloys by making use of the values of $\chi_{orb.}$ and α estimated in § 7.

(1) V^{51} in V–Cr alloys

The composition dependence of the NMR shift of V^{51} in V–Cr alloys[57,58] cannot be explained by the usual theory for the Knight shift.[59] While the values of γ monotonically decrease with increasing concentration of Cr, the NMR shift of V^{51} shows a maximum in $V_{0.4}Cr_{0.6}$ alloy. We make an analysis of NMR shift of V^{51} in V–Cr alloys assuming the following relations between the shift, K_V, and the magnetic susceptibility, χ, following the method of CLOGSTON et al :[60]

$$\left.\begin{aligned} K_V &= K_s + K_d + K_{orb.}, \\ \chi &= \chi_s + \chi_d + \chi_{orb.}, \\ K_s &= a\chi_s, \\ K_d &= b\chi_d, \end{aligned}\right\} \quad (8.1)$$

and

$$K_{orb.} = c\chi_{orb.}$$

where K_s, K_d and $K_{orb.}$ are, respectively, the contribution to NMR shift from the conduction electrons of s-character due to the hyperfine interaction (ordinary Knight shift), from the conduction electrons of d-character due to the exchange polarization of innercore s-electrons and from the conduction electrons of d-character due to the orbital paramagnetism. $\chi_s + \chi_d$ $(=\chi_{spin})$ is the spin paramagnetic susceptibility, where χ_s and χ_d are the spin susceptibilities of the conduction electrons of s-character and of the conduction electrons of d-character, respectively, and $\chi_{orb.}$ is the orbital paramagnetic susceptibility. a, b and c are proportionality constants assumed to be independent of the atomic composition. If we assume that the proportion of the s-character in the band is x for all V–Cr alloys,

that is, $\chi_s = x\chi_{spin}$, then we obtain the relation,

$$K_{spin} = K_s + K_d = \{ax + b(1-x)\}\chi_{spin} \equiv b'\chi_{spin},$$

and Eqs. (8. 1) become

$$\left.\begin{aligned} K_V &= K_{spin} + K_{orb.}, \\ K_{orb.} &= c\chi_{orb.}, \\ &\text{and} \\ K_{spin} &= b'\chi_{spin}. \end{aligned}\right\} \quad (8.\ 1')$$

The value of c is estimated from the relation,

$$c = \frac{2}{L}\xi <r^{-3}>_{atom}, \quad (8.\ 2)$$

where L is Avogadro's number and $\xi = <r^{-3}>_{metal}/<r^{-3}>_{atom}$. In the case where the d-character is predominant and the exchange polarization is large, the value of b' is negative through b. In the other case where the d-character is not predominant and the exchange polarization is not so large, the value of b' may be positive. Also b' can become positive through the fact that the exchange polarization may involve the polarization of s-character conduction electrons in which case b is inherently positive.

By assuming that $<r^{-3}>_{atom} = 2.3$ a. u. [61] and $\xi = 1$, the value of c is estimated as $c = 52$ mole/emu. The values of $\chi_{orb.}$ have been estimated in § 7 (1) a), and the values of χ_{spin} are obtained from the observed values of χ by subtracting the values of $\chi_{orb.}$ ($\chi_{spin} = \chi - \chi_{orb.}$). By making use of these values of χ_{spin} and $\chi_{orb.}$ for V metal and the value of $c = 52$ mole/emu, and by adjusting the value of b' to make agree the calculated values of K_V with the experimental value in V metal, we obtain the value of $b' = -30.6$ mole/emu. Using the values of $b' = -30.6$ mole/emu, $c = 52$ mole/emu, $\chi_{orb.}$ for each composition of alloys estimated in § 7 (1) a) and observed χ, [29~31] we calculate the value of K_V in V–Cr alloys. The calculated results well explain the experimental results [57, 58] as shown in Table 8 and in Fig. 75. Each of K_{spin}, $K_{orb.}$ and K_V is shown in Fig. 76. It is seen from this figure that the contribution of the orbital paramagnetism is most dominant. The fact that $K_{spin} < 0$ means K_d is more dominant than K_s. It will be concluded that the NMR shift of V^{51} in V metal and V–Cr alloys are mainly determined by positive $K_{orb.}$ and negative K_{spin}, and the increase of K_V from V metal to $V_{0.4}Cr_{0.6}$ alloy is attributable to the decrease of the absolute value of K_{spin} due to the decrease of χ_{spin}, and the decrease of K_V from $V_{0.4}Cr_{0.6}$ alloy to more Cr rich alloy is attributable to the decrease of $K_{orb.}$ due to the decrease of $\chi_{orb.}$.

Table 8 The NMR shifts of V^{51} in V metal and V–Cr alloys, K_V, and the contributions to K_V from conduction electrons due to hyperfine interaction and exchange polarization, K_{spin}, and due to orbital paramagnetism, $K_{orb.}$. Also magnetic susceptibilities are shown. $\chi_{obs.}$ and $\chi_{orb.}$ are, respectively, observed values of magnetic susceptibilities, and values of orbital paramagnetic susceptibilities estimated in § 7 (1) (the values marked by * are interpolated ones). χ_{spin} is the spin susceptibility obtained by $\chi_{spin} = \chi_{obs.} - \chi_{orb.}$. Both calculated and observed values of K_V are shown. Here, the parameters are chosen as follows : $c = 52$ mole/emu and $b' = -30.6$ mole/emu. Observed values of χ are quoted from references 28~31. Observed values of K_V are quoted from references 57 and 58.

Composition	$\chi_{obs.}$	$\chi_{orb.}$	χ_{spin}	K_{spin}	$K_{orb.}$	K_V (calc.)	K_V (obs.)	K_V (obs.)
	10^{-4} emu/mole			%		%	%	
V	2.96	1.78	1.18	−0.361	0.926	0.565	0.565	0.565
$V_{0.9}Cr_{0.1}$	2.84	1.74*	1.10	−0.336	0.905	0.569	0.565	—
$V_{0.85}Cr_{0.15}$	2.69	1.72*	0.97	−0.297	0.894	0.597	—	—
$V_{0.8}Cr_{0.2}$	2.78	1.70*	1.08	−0.330	0.884	0.554	0.591	0.600
$V_{0.75}Cr_{0.25}$	2.61	1.70	0.91	−0.278	0.884	0.606	—	—
$V_{0.7}Cr_{0.3}$	2.57	1.70*	0.87	−0.266	0.884	0.618	0.588	0.619
$V_{0.6}Cr_{0.4}$	2.46	1.70*	0.76	−0.233	0.884	0.651	0.612	—
$V_{0.5}Cr_{0.5}$	2.44	1.70	0.74	−0.226	0.884	0.658	0.647	0.663
$V_{0.5}Cr_{0.5}$	2.39	1.70	0.69	−0.211	0.884	0.673	0.647	0.663
$V_{0.4}Cr_{0.6}$	2.08	1.60*	0.48	−0.147	0.832	0.685	0.671	0.688
$V_{0.3}Cr_{0.7}$	1.85	1.50*	0.35	−0.107	0.780	0.673	0.669	0.671
$V_{0.25}Cr_{0.75}$	1.72	1.45	0.27	−0.083	0.754	0.671	—	—
$V_{0.2}Cr_{0.8}$	—	—	—	—	—	—	0.623	0.631
$V_{0.1}Cr_{0.9}$	1.83	1.39*	0.44	−0.135	0.723	0.588	0.589	—
$V_{0.05}Cr_{0.95}$	1.77	1.37*	0.40	−0.122	0.712	0.590	0.567	—
$Cr_{1.0}V_{0.0}$	1.74	1.35	0.39	−0.119	0.702	0.583	0.551	—
$Cr_{1.0}V_{0.0}$	1.65	1.35	0.30	−0.092	0.702	0.610	0.551	—

(2) Nb^{93} and Tc^{99} in Nb–Mo and Nb–Tc alloys

We make an analysis of NMR shifts, K_{Nb} and K_{Tc}, of Nb^{93} in Nb–Mo alloys[62] and of Nb^{93} and Tc^{99} in Nb–Tc alloys.[49] Relations similar to Eqs. (8. 1′) are assumed for K_{Nb} and K_{Tc}. From spin-orbit interaction in atoms of 4d transition elements SHIMIZU[63] estimated that $(2/L)\langle r^{-3}\rangle_{atom} = 96.82$ mole/cm^3 for Nb, 120.2 mole/cm^3 for Mo and 147.1 mole/cm^3 for Tc.

For Nb^{93} in Nb metal using the value of $c = 95$ mole/emu ($\xi \approx 1$) and the values of $\chi_{orb.}$ and χ_{spin} estimated in § 7 (3) a) and adjusting the value of b' to get good agreement between calculated and experimental values of K_{Nb}, we obtain $b' = -8.71$ mole/emu. The calculated values of K_{Nb} in Nb–Mo and Nb–Tc alloys by making use of the values of $b' = -8.71$ mole/emu, $c = 95$ mole/emu and the

Table 9 The NMR shifts of Nb^{93} and Tc^{99} in Nb–Mo and Nb–Tc alloys, K_{Nb} and K_{Tc}, and the contributions from the orbital paramagnetism of d-electrons, $K_{orb.}$ and from the exchange polarization and the hyperfine interaction, K_{spin}. Also the estimated values of $\chi_{orb.}$ and χ_{spin} are shown. Both calculated and observed values of K_{Nb} and K_{Tc} are shown. Here, the parameters are chosen as follows : $c(Nb) = 95$ mole/emu, $b'(Nb) = -8.71$ mole/emu, and $c(Tc) = 100$ mole/emu, $b'(Tc) = +9.45$ mole/emu. Observed values in Nb–Mo alloys under $H = 15$ KOe are marked by * (reference 62) and those in Nb–Tc alloys under $H = 14$ KOe are marked by ** (reference 49).

e/a	$\chi_{orb.}$	χ_{spin}	Nb^{93} (calc.)			Nb^{93} (exp.)		Tc^{99} (calc.)			Tc^{99} (exp.)
	10^{-4} emu/mole		$K_{orb.}$	K_{spin}	K_{Nb}	K_{Nb}*	K_{Nb}**	$K_{orb.}$	K_{spin}	K_{Tc}	K_{Tc}**
			%			%		%			%
5.0(Nb)	0.980	1.159	0.931	−0.101	0.830	0.83	0.821	(0.980)	(+0.110)	(1.090)	—
5.1	0.968	1.153	0.920	−0.100	0.820	0.80	—	0.968	+0.109	1.077	—
5.2	0.950	1.143	0.903	−0.100	0.803	—	0.801	0.950	+0.108	1.058	1.058
5.225	—	—	—	—	—	0.81	—	—	—	—	—
5.25	0.940	1.138	0.893	−0.099	0.794	—	—	0.940	+0.108	1.048	—
5.3	0.929	1.090	0.883	−0.095	0.788	—	—	0.929	+0.103	1.032	—
5.375	—	—	—	—	—	0.83	—	—	—	—	—
5.4	0.896	0.685	0.851	−0.060	0.791	—	0.791	0.896	+0.065	0.961	0.970
5.5	0.850	0.286	0.808	−0.025	0.783	0.80	—	0.850	+0.027	0.877	—
5.6	0.762	0.251	0.724	−0.022	0.702	0.69	0.699	0.762	+0.024	0.786	0.780
5.65	—	—	—	—	—	0.73	—	—	—	—	—
5.7	0.683	0.230	0.649	−0.020	0.629	0.68	—	0.683	+0.022	0.705	—
5.75	0.660	0.226	0.627	−0.020	0.607	0.66	—	0.660	+0.021	0.681	—
5.8	0.640	0.228	0.608	−0.020	0.588	0.68 0.64	—	0.640	+0.022	0.662	—
5.85	—	—	—	—	—	0.615	—	—	—	—	—
5.9	0.615	0.245	0.584	−0.021	0.563	0.615	—	0.615	+0.023	0.638	—
5.95	—	—	—	—	—	0.58 0.57 0.55	—	—	—	—	—
6.0(Mo)	0.600	0.280	0.570	−0.024	0.546	—	0.601	0.600	+0.026	0.626	0.546

values of $\chi_{orb.}$ and χ_{spin} estimated in § 7 (3) a), are shown in Table 9 and in Fig. 77 (curve (1)), where it was assumed that the values of $\chi_{orb.}$ and χ_{spin} are common, respectively, for Nb–Mo and Nb–Tc alloys with common value of e/a. The curve of calculated result is very similar to the experimental curves. A disagreement between calculated and experimental results appears in Mo rich (or Tc rich) range where $e/a > 5.7$. This disagreement may be attributed to the assumption that the value of c is independent of the atomic composition. As a matter of fact, the values of c may change with the atomic composition. If the constituent atoms of an alloy have a tendency to adapt themselves to the surroundings and to have similar values of $\langle r^{-3} \rangle_{metal}$, we may make use of a larger value of c,

for example, $c=105$ mole/emu in the Mo rich alloy. If it is so, the disagreement in the Mo rich range disappears (curve (1')).

Such a behaviour of atoms in an alloy may make the value of c of Tc in the Nb rich alloy smaller than the value estimated for the Tc atom. By assuming $c=100$ mole/emu ($\xi\approx 0.68$) and $b'=+9.45$ mole/emu for Tc in Nb–Tc alloys, which are obtained by trial and error calculation, and using the value of $\chi_{\text{orb.}}$ and χ_{spin} estimated in § 7 (3) a), we obtain the value of K_{Tc} in Nb–Tc alloys as shown in Table 9 and in Fig. 78 (curve (1)). A good agreement between the calculated and experimental result is obtained. It should be noted that the value of b' is positive in this case.

A value of ξ less than unity means an expansion of the d-orbit in the metal. This may arise from an increase of the number of s-character conduction electrons which screen the excess charge of the atomic core of impurity atom. In this case, the positive contribution to b' will increase and the negative one will decrease. This consideration is consistent with the fact that $\xi=0.68<1$ and $b'>0$ for Tc in Nb rich Nb–Tc alloys. The sign of b' is closely related to the shape of the K–e/a curve. For Nb^{93} with $b'<0$, the decrease of $K_{\text{orb.}}$ due to decrease of $\chi_{\text{orb.}}$ and the increase of K_{spin} due to the decrease of χ_{spin} almost cancel each other and the curve of $K_{\text{Nb}}-e/a$ is relatively flat in Nb rich range. On the other hand, for Tc^{99} with $b'>0$, the decrease of $K_{\text{orb.}}$ due to the decrease of $\chi_{\text{orb.}}$ and the decrease of K_{spin} due to the decrease of χ_{spin} are added together and the curve of $K_{\text{Tc}}-e/a$ sharply decrease with increasing concentration of Tc in the Nb rich range. If we make use of an ordinary negative value of b', for example, $b'=-7.17$ mole/emu and a value of $c=120$ mole/emu, we obtain the curve (1') in Fig. 78 which does not agree with the experimental curve satisfactorily.

The analysis on K_{Nb} in Nb metal is compared with that on the NMR shift of V^{51}, K_{V}, in V metal. The value of $\chi_{\text{orb.}}=1.78\times 10^{-4}$ emu/mole for V metal is larger than that of $\chi_{\text{orb.}}=0.98\times 10^{-4}$ emu/mole for Nb metal, while the value of $c=52$ mole/emu for V^{51} is smaller than that of $c=95$ mole/emu for Nb^{93}, then the values of $K_{\text{orb.}}$ are almost equal to each other ($K_{\text{orb.}}$ (V) $=0.926\%$, $K_{\text{orb.}}$ (Nb) $=0.931\%$). On the other hand, the values of χ_{spin} for V and Nb metals are almost equal to each other (χ_{spin} (V) $=1.18\times 10^{-4}$ emu/mole, χ_{spin} (Nb) $=1.16\times 10^{-4}$ emu/mole at room temperature), while the absolute value of $b'=-30.6$ mole/emu for V^{51} is larger than that of $b'=-8.71$ mole/emu for Nb^{93}, then the absolute value of K_{spin} for V^{51} is larger than that for Nb^{93} (K_{spin} (V) $=-0.361\%$, K_{spin} (Nb) $=-0.101\%$). Finally, K_{V} is smaller than K_{Nb} ($K_{\text{V}}=0.565\%$, $K_{\text{Nb}}=0.830\%$).

In conclusion, by separating χ into χ_{spin} and $\chi_{\text{orb.}}$ and by making use of the proper values of c and b', the NMR shift of Nb^{93} and Tc^{99} in Nb–Mo and Nb–Tc alloys

are satisfactorily explained. The main contribution to these NMR shifts arises from the orbital paramagnetism of d-electrons.

§ 9 Condition of Ferromagnetism

STONER has been shown that the condition of ferromagnetism at 0°K is given by $\alpha > \{2\mu^2\nu(\zeta_0)\}^{-1}$, where μ, α and $\nu(\zeta_0)$ are the Bohr magneton, the molecular field coefficient and the value of the density of states $\nu(\varepsilon)$ at the Fermi level ζ_0 at 0°K for the paramagnetic state.[3] In this case the spin paramagnetic susceptibility χ is given by $\chi = (\chi_0^{-1} - \alpha)^{-1}$, where χ_0 is the spin paramagnetic susceptibility without molecular field. At 0°K, χ_0 is given by $\chi_0(0) = 2\mu^2\nu(\zeta_0)$. If χ_0 decrease monotonically with increasing temperature, as seen in the case of the normal band, and the condition $\alpha > \chi_0(0)^{-1}$ is satisfied, ferromagnetism has appeared at 0°K and there is a Curie temperature, where $\chi_0^{-1} = \alpha$.

In a certain case, where the shape of the density of states curve and the position of the Fermi level are appropriate, χ_0 shows a maximum at a certain temperature, as discussed in § 3 (4) and shown in the calculations on χ_0 in § 5. It seems to be of interest to examine the condition of ferromagnetism by the band model in such a case where the temperature variation of χ_0 shows a maximum and the value of α is smaller than $\chi_0(0)^{-1}$ but larger than the minimum value of χ_0^{-1} as shown schematically in Fig. 79 (a). In this case, as seen from Fig. 79 (a), $\alpha < \chi_0(0)^{-1}$ at 0°K and $\alpha > \chi_0^{-1}$ at the temperatures between T_c' and T_c. At first sight, it may be expected that the metal shows paramagnetism below T_c' and above T_c and shows ferromagnetism at temperatures between T_c' and T_c; it looks as if there exist two Curie temperatures T_c and T_c', and that the temperature dependences of the paramagnetic susceptibility and spontaneous magnetization show behaviours such as shown in Fig. 79 (b). But this is not the case. As a matter of fact, the metal can be ferromagnetic under certain conditions at 0°K even if $\alpha < \chi_0(0)^{-1}$. This conclusion will be explained in the following way.

When the electrons in a band are spontaneously magnetized, we have the following relations among the total energy, the Fermi levels and the spontaneous magnetization, M, at 0°K,

$$\int_{\zeta_-}^{\zeta_0} \nu(\varepsilon)d\varepsilon = \int_{\zeta_0}^{\zeta_+} \nu(\varepsilon)d\varepsilon = M/(2\mu), \tag{9. 1}$$

$$E = \int_{\zeta_0}^{\zeta_+} \varepsilon\nu(\varepsilon)d\varepsilon - \int_{\zeta_-}^{\zeta_0} \varepsilon\nu(\varepsilon)d\varepsilon - \frac{1}{2}\alpha M^2, \tag{9. 2}$$

and

$$\zeta_+ - \zeta_- = 2\mu\alpha M, \tag{9. 3}$$

where E is the total energy in the magnetized state at 0°K, and ζ_+, ζ_- and ζ_0 are the Fermi levels of plus and minus spin subbands in a magnetized state and the Fermi level in the non-magnetized state, respectively. The condition (9.3) is equivalent to the condition,

$$dE/dM = 0 \tag{9.3'}$$

(cf. Appendix II (1)).

The condition $\alpha > \{2\mu^2\nu(\zeta_0)\}^{-1}$ given by STONER[3] is equivalent to the condition $(d^2E/dM^2)_{M=0} < 0$ (cf. Appendix II (2)). This means that the solution $M=0$ is an unstable solution and the energy of a ferromagnetic solution $M \neq 0$ become lower than the energy of the state $M=0$. If this condition is satisfied, the metal becomes ferromagnetic at any rate. Therefore, STONER's condition is a sufficient condition of ferromagnetism for the electrons in the band. But this condition is not always a necessary one.

For a density of states curve shown schematically in Fig. 79 (c), it is expected the temperature variation of χ_0 is similar to that shown in Fig. 79 (a), showing a maximum at a certain temperature. In this case, even if $\alpha < \chi_0(0)^{-1}$ (this means that $(d^2E/dM^2)_{M=0} > 0$, that is, the solution $M=0$ is a stable solution), if α is not too small, there can be another stable solution $M \neq 0$ and it is expected that the dependence of E on M is shown by a curve such as shown schmatically in Fig. 79 (d). It depends on the detailed shape of the density of states curve, the position of the Fermi level and the value of α whether the energy at the right-hand minimum where $M \neq 0$ is lower or higher than that at the left-hand minimum where $M=0$ in Fig. 79 (d). Then, if the shape of the density of states curve, the position of the Fermi level and the value of α are appropriate, there is a possibility of ferromagnetism of electrons in a metal even if $\alpha < \chi_0(0)^{-1}$, that is, Eqs. (9.1), (9.2) and (9.3) have a solution, $M \neq 0$ and $E < 0$.

In order to illustrate this possibility of ferromagnetism where $\alpha < \chi_0(0)^{-1}$, we consider a simple example where the density of states is given by $\nu(\varepsilon) = a + b\varepsilon^2$ with $a > 0$ and $b > 0$, and where we choose $\zeta_0 = 0$. In this case, $\zeta_+ = -\zeta_- \equiv \zeta$, $M = 2\mu\{a\zeta + (b/3)\zeta^3\}$ and $E = (1 - 2\alpha\mu^2 a)a\zeta^2 + \{\frac{1}{2} - (4/3)a\alpha\mu^2\}b\zeta^4 - (2\alpha\mu^2/9)b^2\zeta^6$. In the limiting case where $M \to 0$, we have $E = \{1 - 2\alpha\mu^2\nu(0)\}\nu(0)\zeta^2$ using $\nu(0) = a$. If $\alpha < \{2\mu^2\nu(0)\}^{-1}$, the solution $M=0$ is a stable solution. If, however, M is sufficiently large, E becomes negative because of the term proportional to ζ^6. In this case, the energy of the ferromagnetic state with $M \neq 0$ can at any rate be lower than the non-magnetized state with $M=0$, although there may be no minimum of the energy at $M \neq 0$ (the broken line in Fig. 79 (d)) because the band assumed here is an open band. If, however, the band is closed as shown in Fig. 79 (c),

there is a limited range of M, and E may increase again at larger values of M. We then will have a stable ferromagnetic state even if $\alpha < \chi_0(0)^{-1}$, if α is not too small.

It is concluded that there are certain possibilities of ferromagnetism in the band model, even if $\alpha < \chi_0(0)^{-1}$, if the shape of the density of states curve, the position of the Fermi level and the values of α are appropriate.

§ 10 Summary

It has been shown that the temperature variation of electronic specific heats of transition metals shows a behaviour to be consistent with the correlation between magnitude of $\gamma(0)$ and χ and the sign of $d\chi/dT$, to be interpretable by the band model and to support an interpretation based on the band model.

Calculated results obtained by making use of the density of states curves determined from the low temperature specific heat data of several series of transition metals and their alloys, have well explained the behaviour of the temperature variation of electronic specific heats of the transition metals. This fact seems to mean that the density of states curves used in the calculations are very close to those of the real metals. We have estimated values of the molecular field coefficient, α, and of the orbital paramagnetic susceptibility, $\chi_{\text{orb.}}$, for transition metals and alloys. Using the values of $\chi_{\text{orb.}}$ and α estimated and the values of χ_0 calculated, we have explained the composition dependence of NMR shift in several alloy systems, which cannot be explained by the usual theory of the Knight shift.

Examining the condition of ferromagnetism, we have shown that there are certain possibilities of ferromagnetism in the band model, even if STONER's condition is not satisfied, if the shape of the density of states curve, the position of the Fermi level and the value of α are appropriate.

Acknowledgment

The author wishes to express his hearty thanks to Prof. SHIMIZU for obliging guidance and directive discussions, and to Dr. TAKAHASHI for constant encouragement and valuable discussions.

Some parts of this work have been published in the following articles by SHIMIZU, TAKAHASHI and KATSUKI : J. Phys. Soc. Japan **17** (1962) 1740 ; **18** (1963) 240, 801, 1192, 1744 ; **19** (1964) 1135, 1856 ; Physics Letters 8 (1964) 7 ; Proc. Int. Conf. on Magnetism, Nottingham (1964) 182. Also, see, KATSUKI and SHIMIZU : J. Phys. Soc. Japan **21** (1966) 279, for 5d-b. c. c. system ; and SHIMIZU, KATSUKI and OHMORI : ibid. **21** (1966) 1922, recalculation for 4d-b. c. c. system.

Appendix I

Recently, FISHER[25] omputed C_v from the C_p data of Zr metal by SCOTT (unpublished work quoted by FISHER) by the relation (2. 2) using the observed values of the compressibility, the themal expansion coefficient and the specific volume at each temperature, and he estimated C_D using the Debye temperature of 296°K which was obtained from his data of elastic constant at low temperature. These values of C_v-C_D, which correspond to our C_E, are shown by curve (3) in Fig. 25. To examine the validity of the approximation (2. 3) to the C_p-C_v correction, we have estimated C_p-C_v by the approximation (2. 3) with $a=2.49\times10^{-6}$ mole/cal which is obtained from the values of C_p, β, α_l and V at 300°K used by FISHER, and we have deduced C_v-C_D using FISHER's Θ_D of 296°K. These values of C_v-C_D are also shown by curve (3′) in Fig. 25. Since the curves (3) and (3′) are very close to each other, the approximation (2. 3) to C_p-C_v correction will be valid.

Appendix II

(*1*) From Eq. (9. 1), we have

$$-\mu\int_{\zeta_0}^{\zeta_-}\nu(\varepsilon)d\varepsilon=\mu\int_{\zeta_0}^{\zeta_+}\nu(\varepsilon)d\varepsilon=M/2. \tag{AII. 1}$$

Therefore,

$$d(M/2)/d\zeta_\pm=\pm\mu\nu(\zeta_\pm). \tag{AII. 2}$$

From Eqs. (9. 2) and (AII. 2)

$$\begin{aligned}dE/dM&=\frac{d\zeta_+}{dM}\zeta_+\nu(\zeta_+)+\frac{d\zeta_-}{dM}\zeta_-\nu(\zeta_-)-\alpha M\\&=(2\mu)^{-1}\{(\zeta_+-\zeta_-)-2\mu\alpha M\}.\end{aligned} \tag{AII. 3}$$

Therefore, in the case of (9. 3′) we have (9. 3).

(*2*) Differentiating (AII. 3) with M and using (AII. 2), we have

$$\begin{aligned}d^2E/dM^2&=(2\mu)^{-1}\left\{\frac{d\zeta_+}{dM}-\frac{d\zeta_-}{dM}-2\mu\alpha\right\}\\&=(2\mu)^{-1}\left[\{2\mu\nu(\zeta_+)\}^{-1}+\{2\mu\nu(\zeta_-)\}^{-1}-2\mu\alpha\right].\end{aligned}$$

Then,

$$(d^2E/dM^2)_{M=0}=\{2\mu^2\nu(\zeta_0)\}^{-1}-\alpha. \tag{AII. 4}$$

From this, if $\alpha>\{2\mu^2\nu(\zeta_0)\}^{-1}$, $(d^2E/dM^2)_{M=0}<0$.

References

1) Stoner, E. C. (1954) Acta Metallurgica, **2**, 259.
2) Shimizu, M. and Takahashi, T. (1960) J. Phys. Soc. Japan, **15**, 2236; (1961) *ibid.* **16**, 1544.
3) Stoner, E. C. (1936) Proc. Roy. Soc. A, **154**, 656.
4) Kubo, R. and Obata, Y. (1956) J. Phys. Soc. Japan **11**, 547.
5) Nernst, W. and Lindemann, F. A. (1911) Z. Elektrochem., **17**, 817.
6) American Institute of Physics Handbook, 2nd edition (McGraw-Hill Book Comp., Inc., New York, 1963) 4–66.
7) Bridgman, P. W. (1958) The Physics of High Pressure (G. Bell and Sons Ltd., London) 160.
8) American Institute of Physics Handbook, 2nd edition (McGraw-Hill Book Comp., Inc., New York, 1963) 4–48.
9) Hoare, F. E., Matthews, J. C. and Walling, J. C. (1953) Proc. Roy. Soc. A, **216**, 502.
10) Cheng, C. H., Gupta, K. P., Van Reauth, E. C. and Beck, P. A. (1962) Phys. Rev., **126**, 2030.
11) Cheng, C. H., Wei, C. T. and Beck, P. A. (1960) Phys. Rev., **120**, 426.
12) Estermann, I., Friedberg, S. A. and Goldman, J. E. (1952) Phys. Rev., **87**, 582.
13) Bozorth, R. M. (1951) Ferromagnetism (D. Van Nostrand Comp., Inc., New York) 441.
14) Wolcott, N. M. (1957) Phil. Mag., **2**, 1246.
15) Montgomery, H. and Pells, G. P. (1961) Proc. Phys. Soc., **78**, 622.
16) Roberts, L. M. (1958) Low Temperature Physics and Chemistry (ed. J. R. Dillinger, The University of Wisconsin Press, Wisconsin) 417.
17) Keeson, W. H. and Kurrelmeyer, B. (1940) Physica, **7**, 1003.
18) Guthrie, G. L., Friedberg, S. A. and Goldman, J. E. (1959) Phys. Rev., **113**, 45.
19) Morin, F. J. and Maita, J. P. (1963) Phys. Rev., **129**, 1115.
20) Daunt, J. G. (1955) Progress in Low Temperature Physics (ed. C. J. Gorter, North-Holland Publishing Company, Amsterdam) 211.
21) Hoare, F. E. and Yates, B. (1957) Proc. Roy. Soc. A, **240**, 42.
22) Budworth, D. W., Hoare, F. E. and Preston, J. (1960) Proc. Roy. Soc. A, **257**, 250.
23) Wolcott, N. M. (1955) Conference de Physique des Basses Temperatures (Suppl. Bull. Inst. Intern. du Froid, Annexe 1955–3) 286.
24) Dixon, M., Hoare, F. E., Holden, T. M. and Moody, D. E. (1963) Pre-Prints of the Sheffield Conference on the Electronic Structure of Alloys, Vol. 1, 1.51.
25) Fisher, S. (1964) Private communication via Shimizu (Read at the Bristol Conference on Solid State Physics).
26) American Institute of Physics Handbook, 1st edition (McGraw-Hill Book Comp., Inc., New York, 1957) 4–40.
27) Lowenthal, G. C. (1963) Australian J. Phys., **16**, 47.
28) Kojima, H., Tebble, R. S. and Williams, D. E. G. (1961) Proc. Roy. Soc. A, **260**, 237.

29) CHILDS, B. G., GARDNER, W. E. and PENFOLD, J. (1960) Phil. Mag., **5**, 1267.
30) TANIGUCHI, S., TEBBLE, R. S. and WILLIAMS, D. E. G. (1962) Proc. Roy. Soc. A, **265**, 502.
31) LINGELBACH, R. (1958) Z. Phys. Chem., **14**, 1.
32) SQUIRE, C. F. and KAUFMANN, A. R. (1941) J. Chem. Phys., **9**, 673.
33) NEWMANN, M. M. and STEVENS, K. W. (1959) Proc. Phys. Soc., **74**, 290.
34) ARROTT, A (1957) Conference on Magnetism and Magnetic Materials (American Institute of Electrical Engineers, New York) 285.
35) TERRY, E. M. (1917) Phys. Rev., **9**, 394.
36) SHIMIZU. M. and KATSUKI, A (1964) Proc. Int. Conf. on Magnetism, Nottingham, 182.
37) FALLOT, M. (1936) Ann. phys., **6**, 305.
38) WEISS, P. and FORRER, R. (1929) Ann. phys., **12**, 279.
39) MEYER, A. J. P. and ASCH, G. (1961) J. Appl. Phys., **32**, 330S.
40) DARKEN, L. S. and SMITH, R. P. (1951) Ind. Eng. Chem., **43**, 1815.
41) FALLOT, M. (1944) J. Phys. radium, **5**, 153.
42) NAKAGAWA, Y. (1956) J. Phys. Soc. Japan, **11**, 855.
43) KAUFMANN, A. R. and STARR, C. (1943) Phys. Rev., **63**, 445.
44) PUGH, E. W. and RYAN, F. M. (1958) Phys. Rev., **111**, 1038.
45) NAKAGOME, R., Private communication.
46) JONES, D. W. and McQUILLAN, A. D. (1962) J. Phys. Chem. Solids, **23**, 1441.
47) MATTHIAS, B. T., PETER, M., WILLIAMS, H. J., CLOGSTON, A. M., CORENZWIT, E. and SHERWOOD, R. C. (1960) Phys. Rev. Letters, **5**, 542.
48) KRIESSMAN, C. J. (1953) Rev. Mod. Phys., **25**, 122.
49) VAN OSTENBURG, D. O., LAM, D. J., SHIMIZU, M. and KATSUKI, A. (1963) J. Phys. Soc. Japan, **18**, 1744.
50) HOARE, F. E. and MATTHEWS, J. C. (1952) Proc. Roy. Soc. A, **212**, 137.
51) WUCHER, M. J. (1952) Ann. Physique, **7**, 317; (1956) Compt. rend., **242**, 1143.
52) RHODES, P. Private communication via SHIMIZU.
53) CRANGLE, J. and SMITH, T. F. (1962) Phys. Rev. Letters **9**, 86.
54) OEHLER, E., Unpublished work as "Staatsexamensarbeit" at Marburg.
55) SHIMIZU, M. and KATSUKI, A (1964) J. Phys. Soc. Japan, **19**, 614.
56) BOZORTH, R. M., DAVIS, D. D. and WERNICK, J. H. (1962) J. Phys. Soc. Japan, **17**, Supplement B-I, 112.
57) BARNES, R. G. and GRAHAM, T. P. (1962) Phys. Rev. Letters, 8, 248.
58) VAN OSTENBURG, D. O., LAM, D. J., TRAPP, H. D. and MACLEOD, D. E. (1962) Phys. Rev., **128**, 1550.
59) KNIGHT, W. D. (1956) Solid State Physics vol. 2 (ed. F. SEITZ and D. TURNBULL, Academic Press Inc., New York) 122.
60) CLOGSTON, A. M., GOSSARD, A. C., JACCARINO, V. and YAFET, Y. (1962) Phys. Rev. Letters, **9**, 262.
61) ABRAGAM, A., HOROWITZ, J. and PRYCE, M. H. L. (1955) Proc. Roy. Soc. A, **230**, 169.
62) ALEXANDER, S., CORENZWIT, E., MATTHIAS, B. T., SHULMAN, R. G. and WYLUDA, B. J. (1963) Phys. Rev., **129**, 2481.
63) SHIMIZU, M., Private communication.

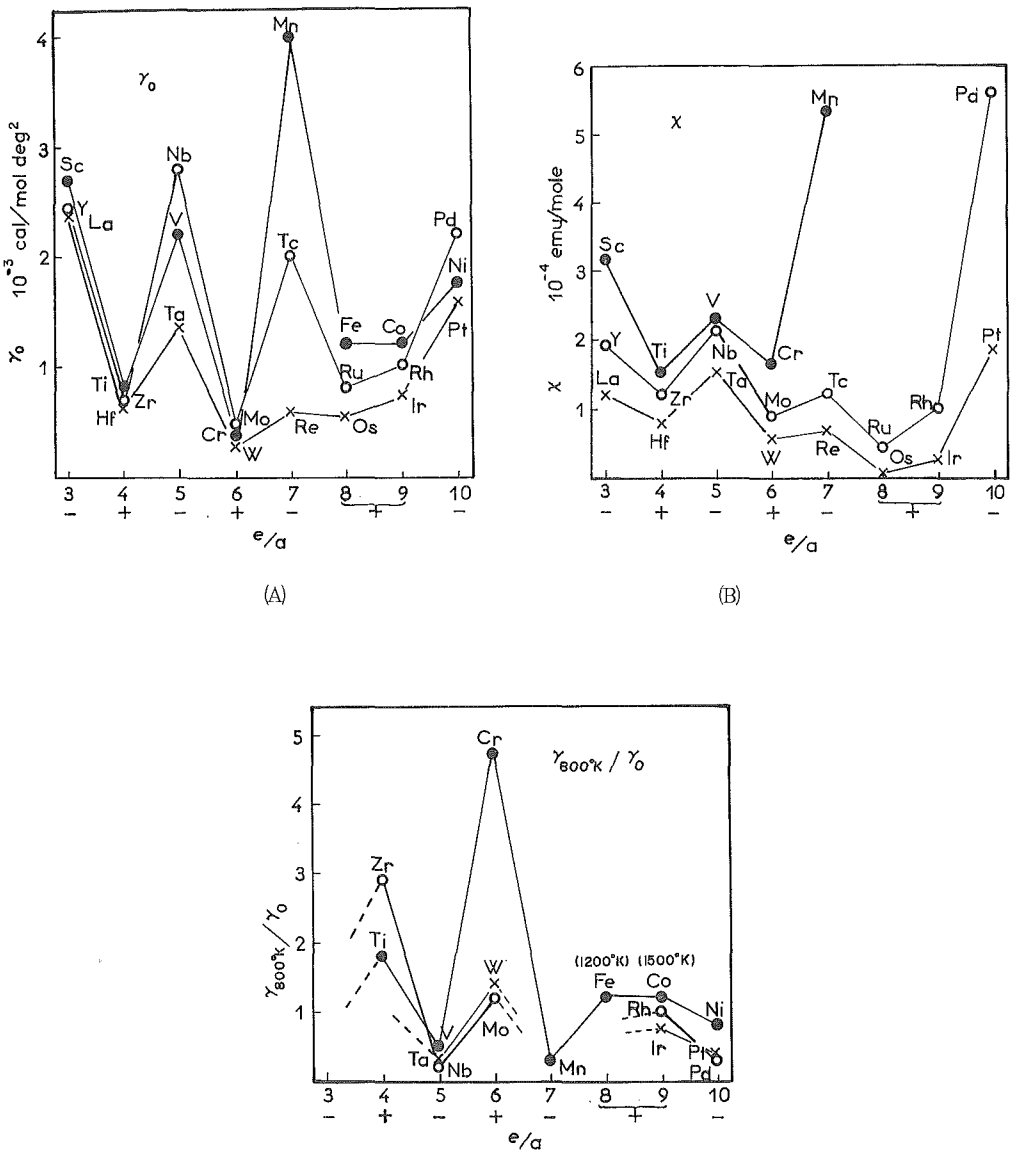

Fig. 1

Fig. 1 Electronic specific heat coefficient, γ, magnetic susceptibility, χ, and temperature variation of the electronic specific heat coefficient in transition metals.

A : Electronic specific heat coefficient at very low temperature, $\gamma(0)$.

B : Magnetic susceptibility, χ.

C : Ratio of γ at 800°K to $\gamma(0)$.

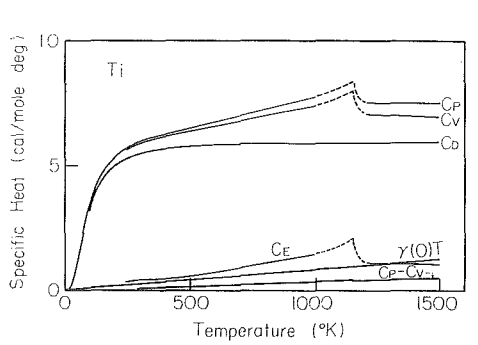
Ti
Specific Heat (cal/mole deg)
10
5
0
0
500
1000
1500
Temperature (°K)
CP
CV
CD
CE
γ(0)T
CP-CV

(A)

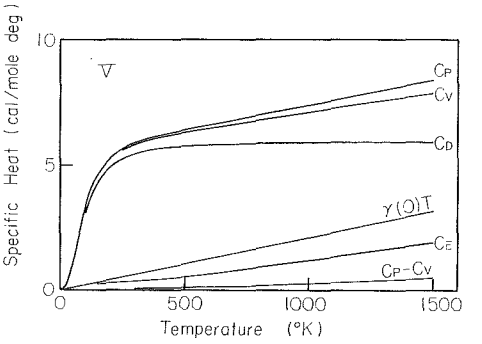
V
Specific Heat (cal/mole deg)
10
5
0
0
500
1000
1500
Temperature (°K)
CP
CV
CD
γ(0)T
CE
CP-CV

(B)

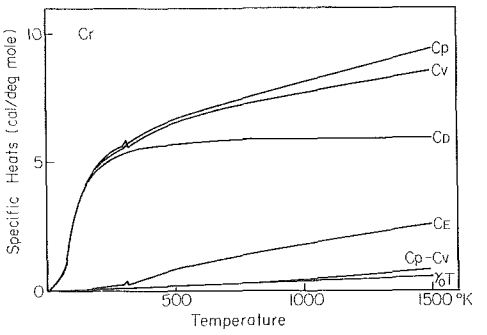
Cr
Specific Heats (cal/deg mole)
10
5
0
500
1000
1500 °K
Temperature
Cp
Cv
CD
CE
Cp-Cv
γT

(C)

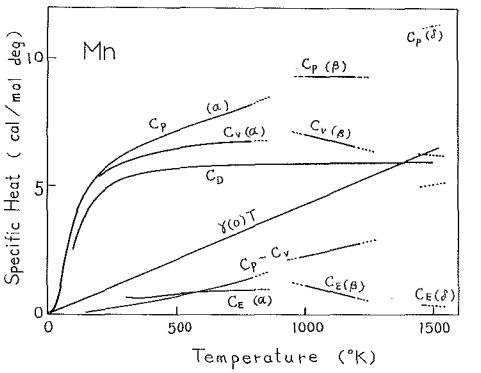
Mn
Specific Heat (cal/mol deg)
10
5
0
0
500
1000
1500
Temperature (°K)
Cp (β)
Cp (α)
Cv (α)
Cv (β)
CD
γ(0)T
Cp - Cv
CE (α)
CE (β)
CE (δ)

(D)

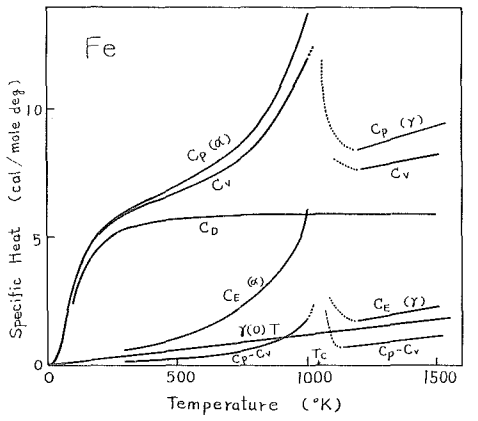
Fe
Specific Heat (cal/mole deg)
10
5
0
0
500
1000
1500
Temperature (°K)
Cp (α)
Cv
Cp (γ)
Cv
CD
CE (α)
CE (γ)
γ(0) T
Cp-Cv
Tc
Cp-Cv

(E)

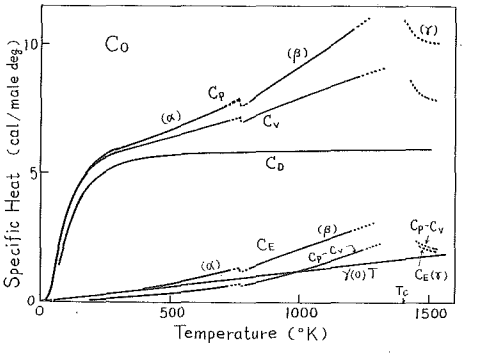
Co
Specific Heat (cal/mole deg)
10
5
0
0
500
1000
1500
Temperature (°K)
(γ)
(β)
Cp
(α)
Cv
CD
CE
(β)
Cp-Cv
(α)
Cp-Cv
γ(0) T
CE(γ)
Tc

(F)

Fig. 2

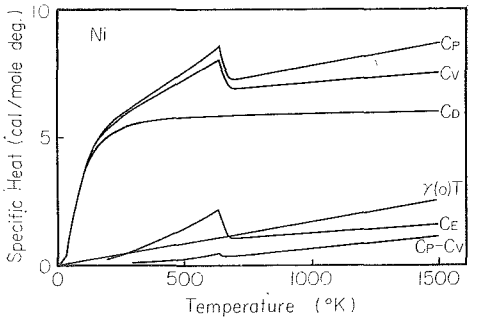
Ni
Cp
Cv
CD
γ(0)T
CE
Cp-Cv
Specific Heat (cal/mole deg.)
Temperature (°K)
0
500
1000
1500
5
10

(G)

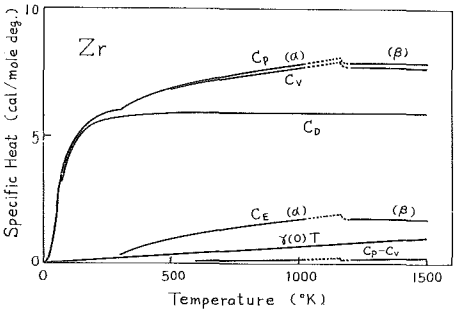
Zr
Cp (α)
(β)
Cv
CD
CE (α)
(β)
γ(0)T
Cp-Cv
Specific Heat (cal/mole deg.)
Temperature (°K)
0
500
1000
1500
5
10

(H)

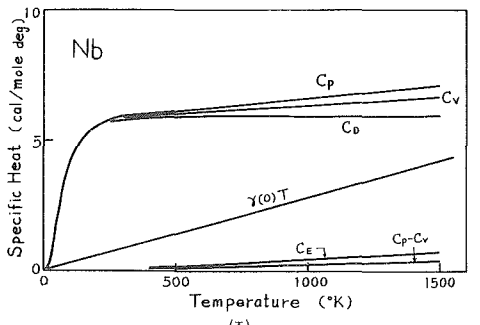
Nb
Cp
Cv
CD
γ(0)T
CE
Cp-Cv
Specific Heat (cal/mole deg.)
Temperature (°K)
0
500
1000
1500
5
10

(I)

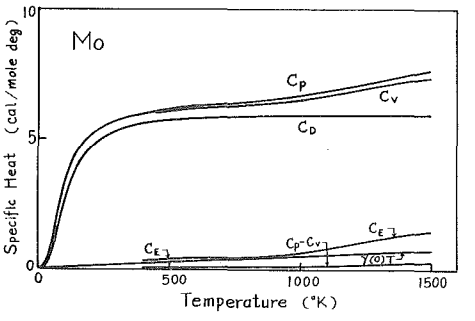
Mo
Cp
Cv
CD
CE
Cp-Cv
γ(0)T
Specific Heat (cal/mole deg.)
Temperature (°K)
0
500
1000
1500
5
10

(J)

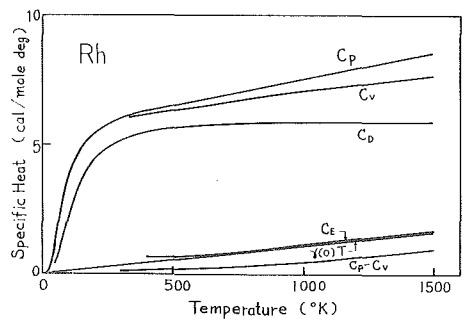
Rh
Cp
Cv
CD
CE
γ(0)T
Cp-Cv
Specific Heat (cal/mole deg.)
Temperature (°K)
0
500
1000
1500
5
10

(K)

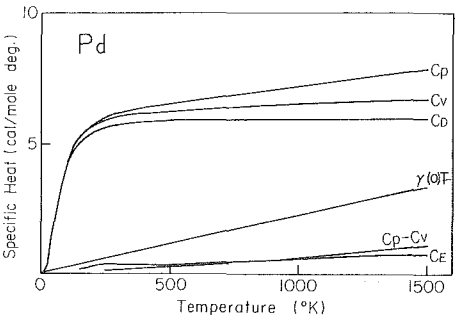
Pd
Cp
Cv
CD
γ(0)T
Cp-Cv
CE
Specific Heat (cal/mole deg.)
Temperature (°K)
0
500
1000
1500
5
10

(L)

Fig. 2

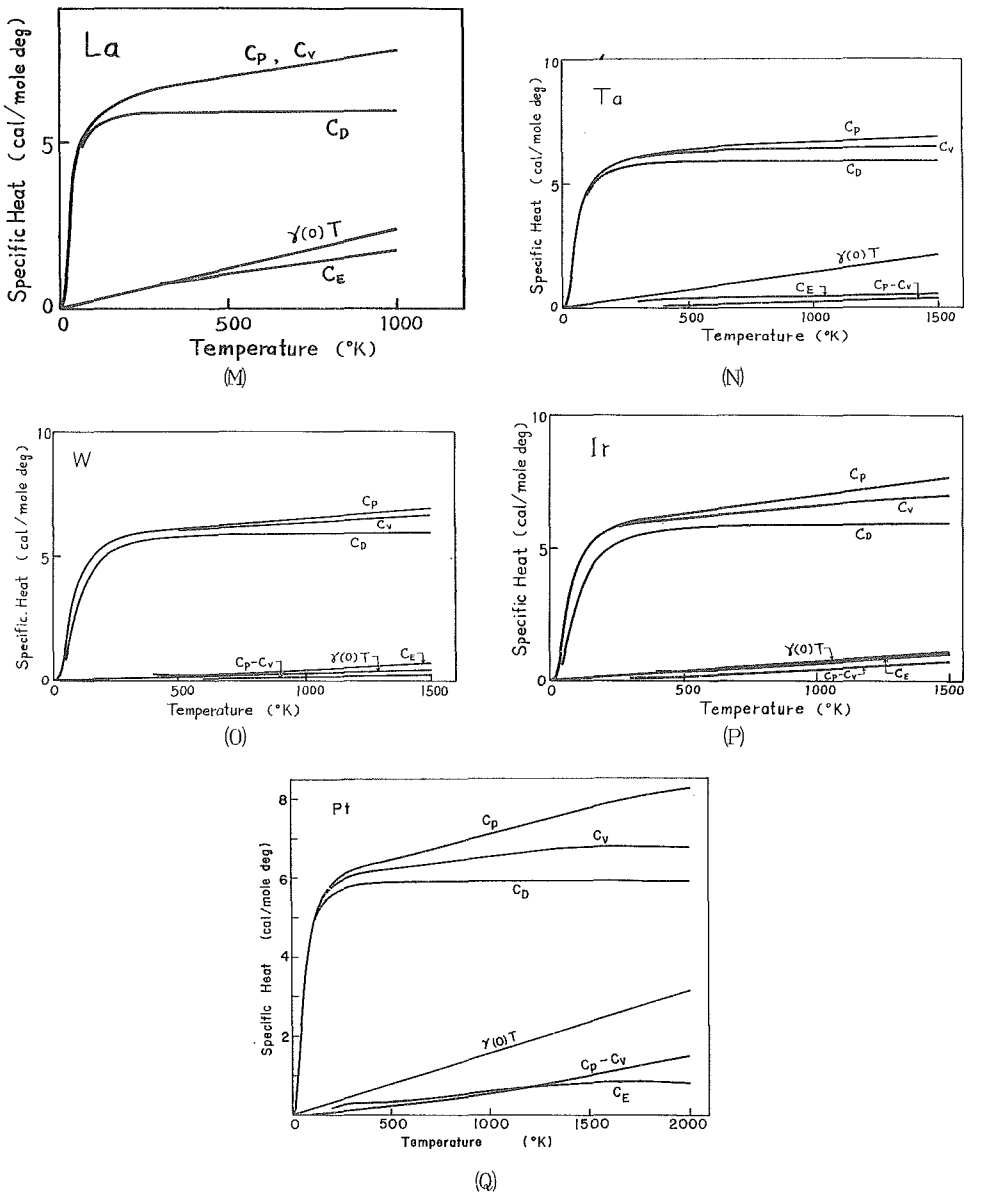

Fig. 2

Fig. 2 Specific heats in transition metals. C_p is observed value at constant pressure. C_v, C_D and C_E are the specific heat at constant volume, the Debye specific heat and the electronic specific heat, respectively. $C_p - C_v$ is the dilatation part. $\gamma(0)T$ is the extrapolation of the electronic specific heat at very low temperature, where the values of $\gamma(0)$ are given in Table 1.

A : Ti, B : V, C : Cr, D : Mn, E : Fe, F : Co, G : Ni, H : Zr, I : Nb, J : Mo, K : Rh, L : Pd, M : La, N : Ta, O : W, P : Ir, Q : Pt.

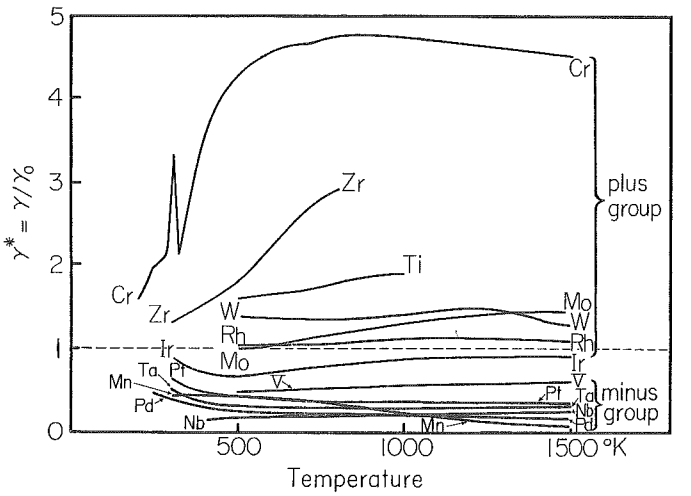

Fig. 3

Fig. 3 Temperature variations of the reduced electronic specific heat coefficient, $\gamma^* \equiv \gamma/\gamma(0)$, for transition metals.

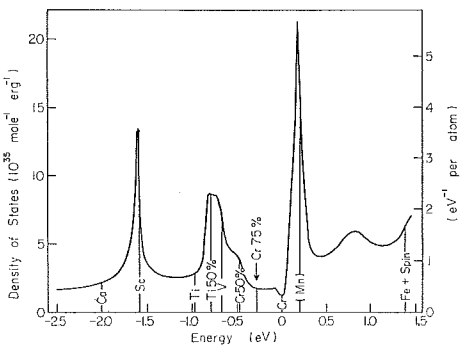

Fig. 4

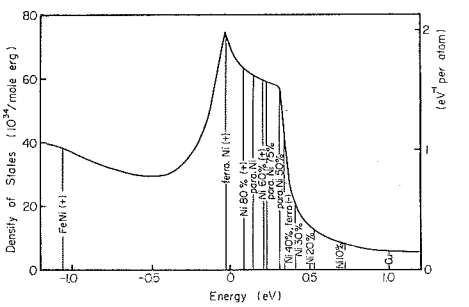

Fig. 5

Fig. 4 Density of states for 3d transition metals and alloys with b. c. c. structure. Fermi levels of the metals and V–Ti and V–Cr alloys are shown. Alloys are specified by the atomic concentration of Ti or Cr.

Fig. 5 Density of states for 3d transition metals and alloys with f. c. c. structure. Fermi levels of the metals and alloys are shown. For ferromagnetics, the Fermi levels of the plus-spin sub-band only are shown, since the Fermi levels of the minus-spin sub-band in the ferromagnetic alloys coincide with that of $Ni_{0.4}\ Cu_{0.6}$ alloy.

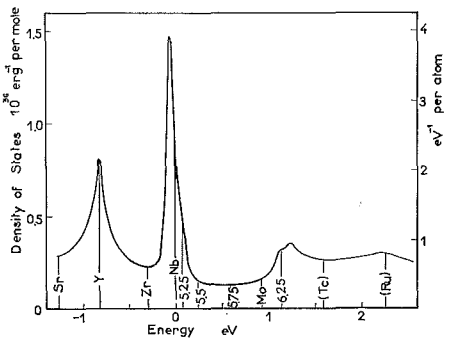

Fig. 6

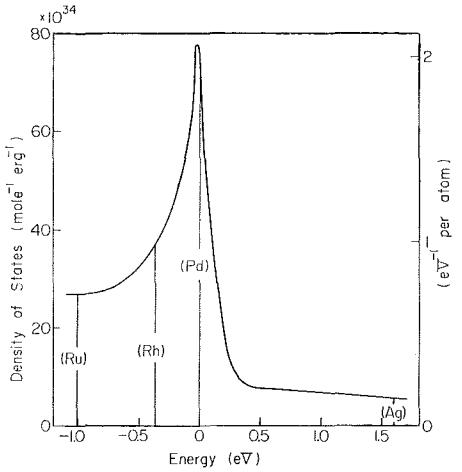

Fig. 7

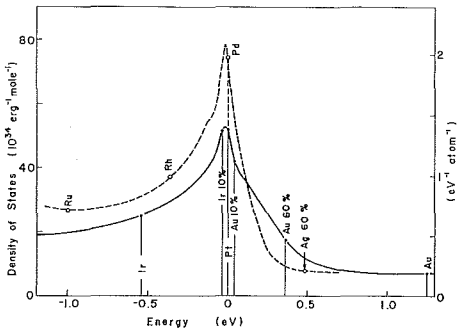

Fig. 8

Fig. 6 Density of states for 4d transition metals and alloys with b.c.c. structure. Fermi levels of the metals and alloys are shown. Alloys are specified by the value of e/a, where $e/a = 5$ for Nb metal and 6 for Mo metal.

Fig. 7 Density of states for 4d transition metals and alloys with f.c.c. structure. Fermi levels of the metals are shown.

Fig. 8 Density of states for 5d transition metals and alloys with f.c.c. structure. Fermi levels of the metals and some Pt alloys are shown. Dashed curve is the density of states for 4d transition metals and alloys with f.c.c. structure.

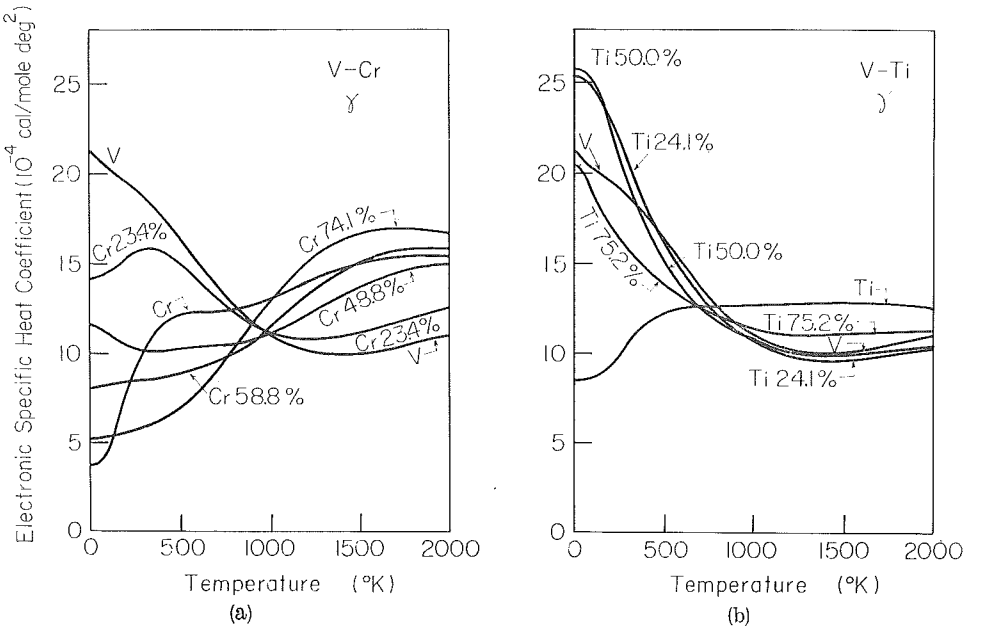

Fig. 9

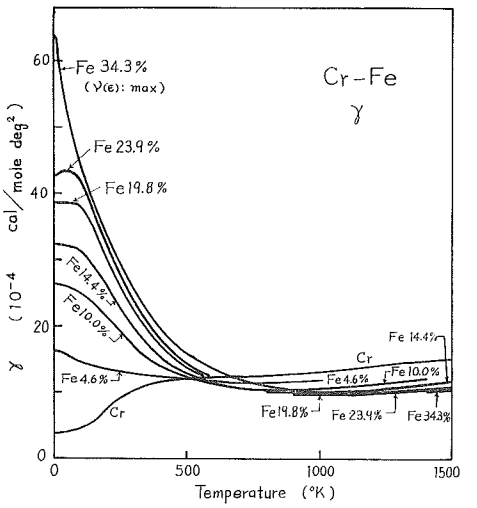

Fig. 10

Fig. 9 Calculated values of the electronic specific heat coefficient for V–Cr and V–Ti alloys.

(a) : V and Cr metals and V–Cr alloys.

(b) : V and Ti metals and V–Ti alloys.

Alloys are specified by the atomic concentration of Cr or Ti.

Fig. 10 Calculated values of the electronic specific heat coefficient for Cr metal and Cr–Fe alloys. Alloys are specified by the atomic concentration of Fe.

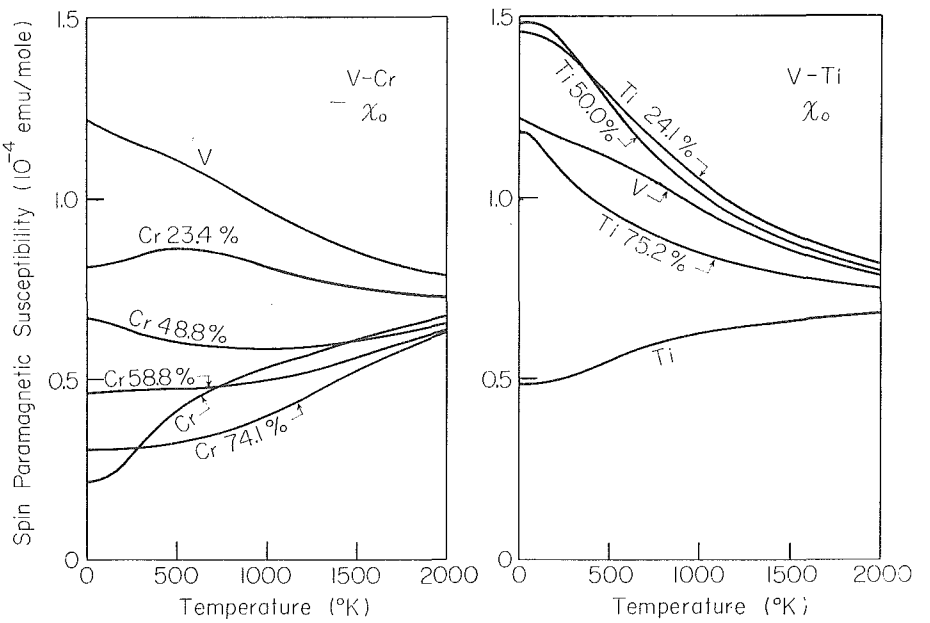

Fig. 11

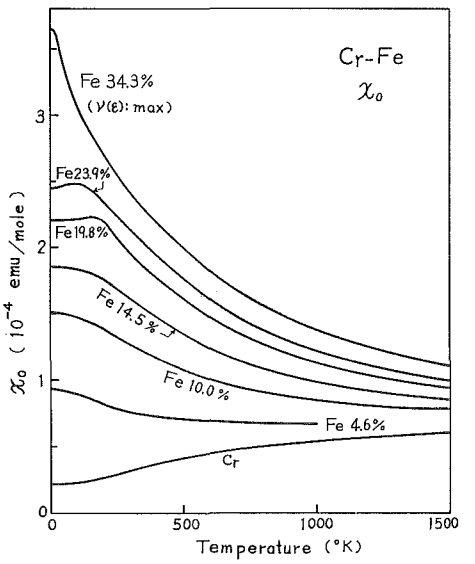

Fig. 12

Fig. 11 Calculated values of the Pauli paramagnetic susceptibility for V–Cr and V–Ti alloys.

(a) : V and Cr metals and V–Cr alloys.

(b) : V and Ti metals and V–Ti alloys.

Fig. 12 Calculated values of the Pauli paramagnetic susceptibility for Cr metal and Cr–Fe alloys. Alloys are specified by the atomic concentration of Fe.

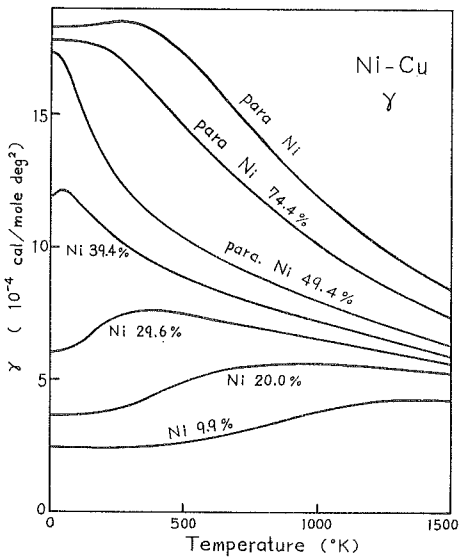

Fig. 13

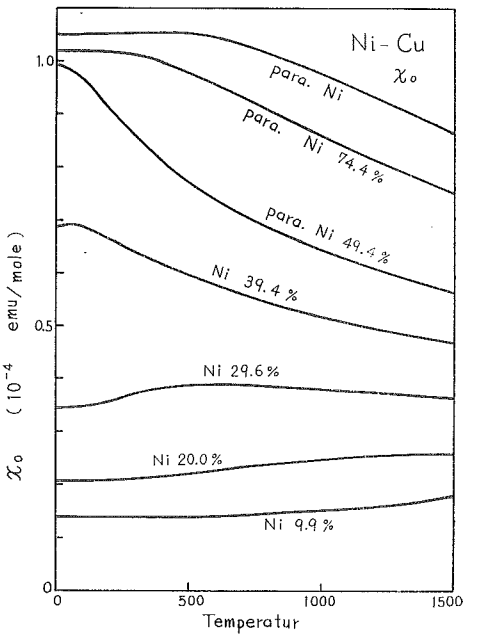

Fig. 14

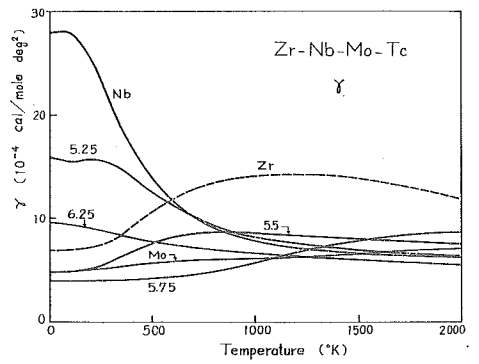

Fig. 15

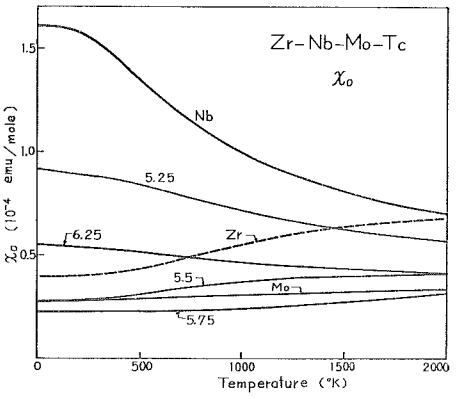

Fig. 16

Fig. 13 Calculated values of the electronic specific heat coefficient for paramagnetic Ni metal and Ni-Cu alloys. Alloys are specified by the atomic concentration of Ni.

Fig. 14 Calculated values of the Pauli paramagnetic susceptibility for paramagnetic Ni metal and Ni-Cu alloys. Alloys are specified by the atomic concentration of Ni.

Fig. 15 Calculated values of the electronic specific heat coefficient for Zr, Nb and Mo metals and their alloys. Alloys are specified by the value of *e/a*.

Fig. 16 Calculated values of the Pauli paramagnetic susceptibility for Zr, Nb and Mo metals and their alloys. Alloys are specified by the values of *e/a*.

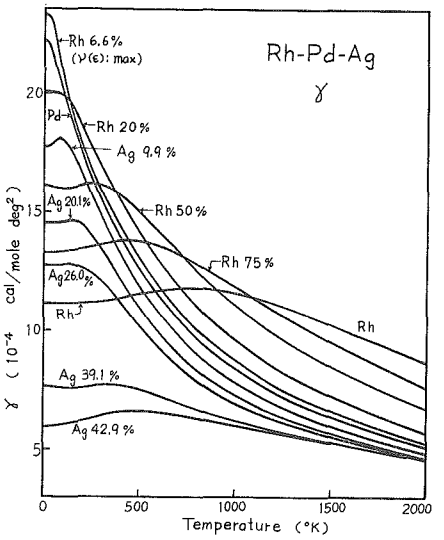

Fig. 17

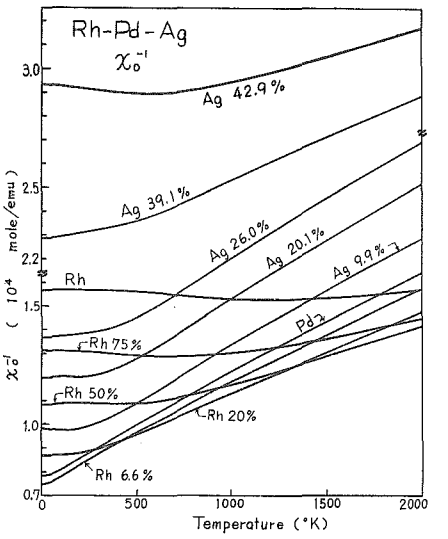

Fig. 18

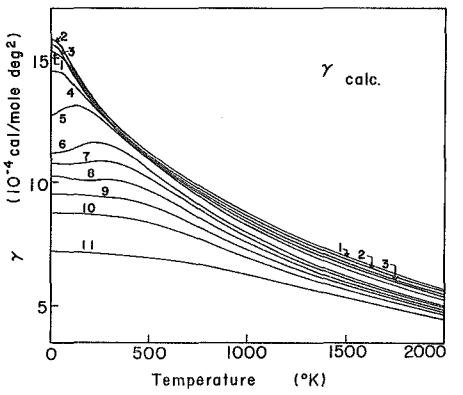

Fig. 19

Fig. 17 Calculated values of the electronic specific heat coefficient for Rh and Pd metals and Pd–Rh and Pd–Ag alloys. Alloys are specified by the atomic concentration of Rh or Ag.

Fig. 18 Calculated values of the reciprocal of the Pauli paramagnetic susceptibility for Rh and Pd metals and Pd–Rh and Pd–Ag alloys. Alloys are specified by the atomic concentration of Rh or Ag.

Fig. 19 Calculated values of the electronic specific heat coefficient for Pt metal and Pt–Ir and Pt–Au alloys.
1 : Ir 10.0% alloy, 2 : Ir 5.6% alloy, 3 : Pt metal, 4 : Au 4.3% alloy,
5 : Au 10.1% alloy, 6 : Au 20.2% alloy, 7 : Au 24.8% alloy, 8 : Au 30.1% alloy,
9 : Au 35.0% alloy, 10 : Au 40.1% alloy, 11 : Au 49.8% alloy.

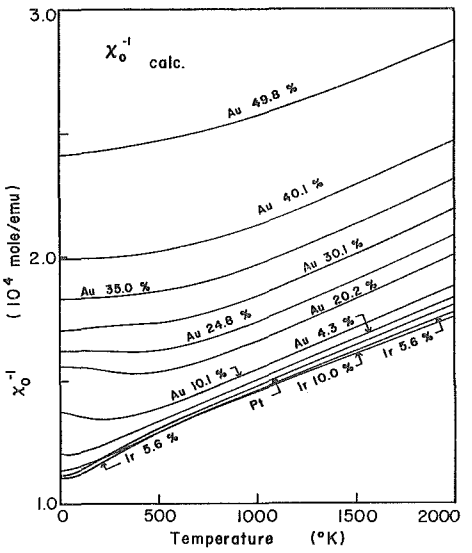

Fig. 20

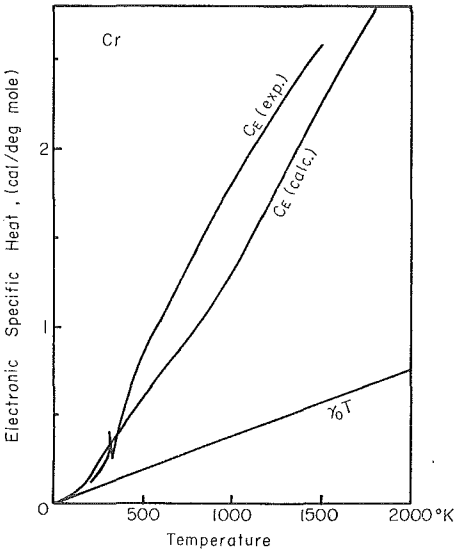

Fig. 21

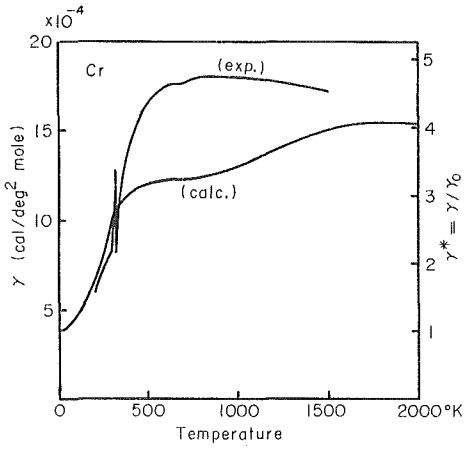

Fig. 22

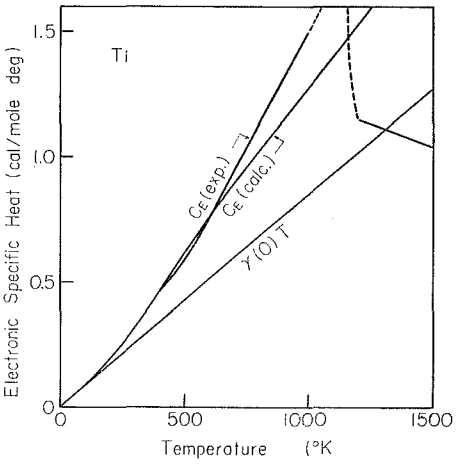

Fig. 23

Fig. 20 Calculated values of the reciprocal of the Pauli paramagnetic susceptibility for Pt metal and Pt–Ir and Pt–Au alloys. Alloys are specified by the atomic concentration of Ir or Au.

Fig. 21 Comparison between temperature variations of the calculated and the experimental electronic specific heat for Cr metal.

Fig. 22 Comparison between temperature variations of the calculated and the experimental electronic specific heat coefficient for Cr metal.

Fig. 23 Comparison between temperature variations of the calculated and the experimental electronic specific heat for Ti metal.

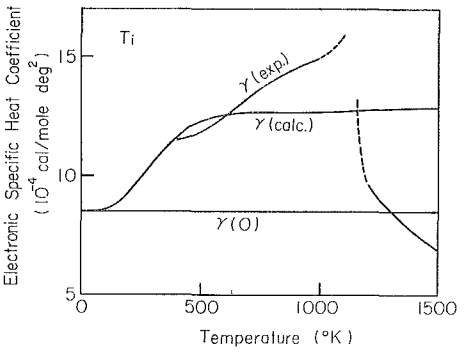

Fig. 24

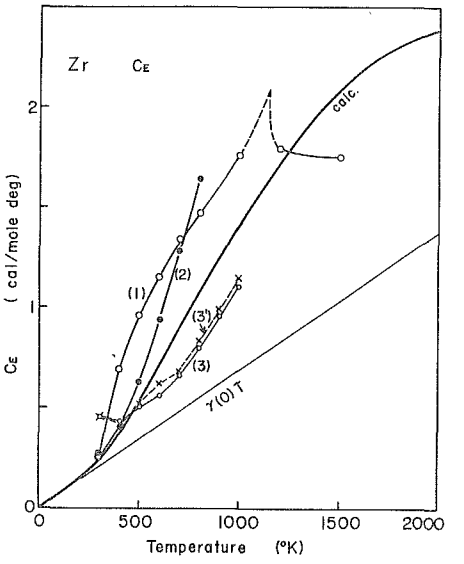

Fig. 25

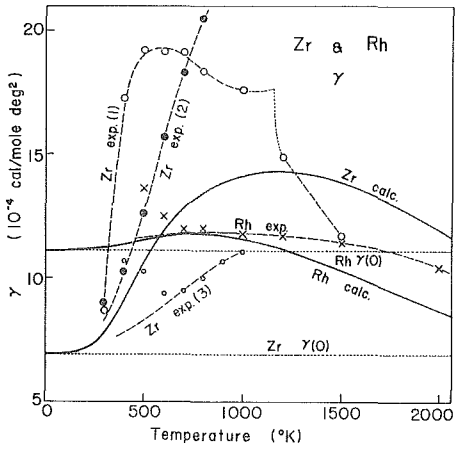

Fig. 26

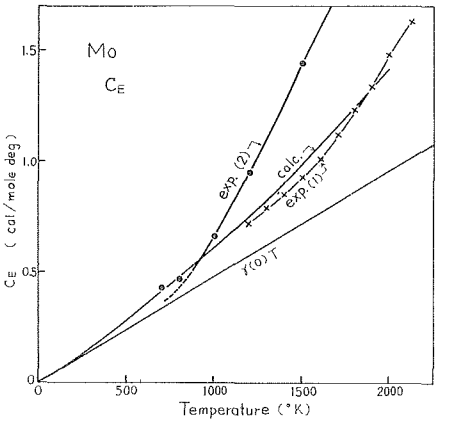

Fig. 27

Fig. 24 Comparison between temperature variations of the calculated and the experimental electronic specific heat coefficient for Ti metal.

Fig. 25 Comparison between temperature variations of the calculated and the experimental electronic specific heat for Zr metal. Experimental values (1), (2), (3) and (3′) are obtained from the data of references 8, 26, and 25, respectively.

Fig. 26 Comparison between temperature variations of the calculated and the experimental electronic specific heat coefficient for Zr and Rh metals. Experimental values for Zr metal, (1), (2), (3) and (3′) are obtained from the data of references 8, 26, and 25, respectively.

Fig. 27 Comparison between temperature variations of the calculated and the experimental electronic specific heat for Mo metal. Experimental values (1) and (2) are obtained from the data of references 27 and 8, respectively.

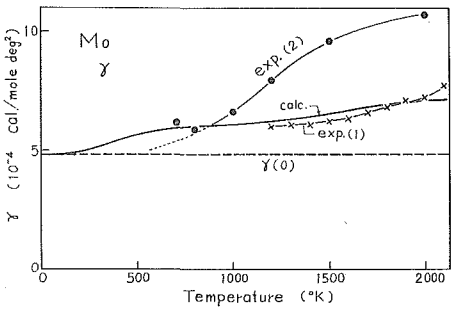

Fig. 28

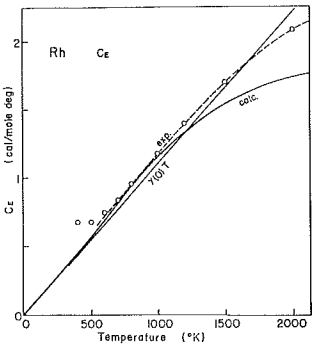

Fig. 29

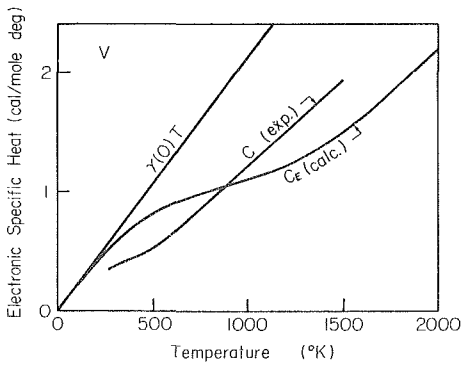

Fig. 30

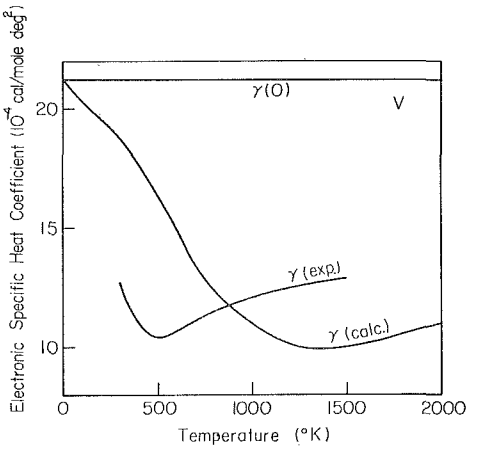

Fig. 31

Fig. 28 Comparison between temperature variations of the calculated and the experimental electronic specific heat coefficient for Mo metal. Experimental values (1) and (2) are obtained from the data of references 27 and 8, respectively.

Fig. 29 Comparison between temperature variations of the calculated and the experimental electronic specific heat for Rh metal.

Fig. 30 Comparison between temperature variations of the calculated and the experimental electronic specific heat for V metal.

Fig. 31 Comparison between temperature variations of the calculated and the experimental electronic specific heat coefficient for V metal.

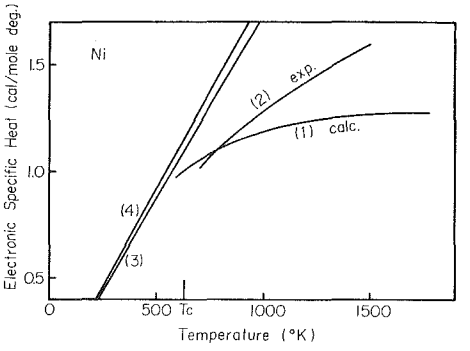

Fig. 32

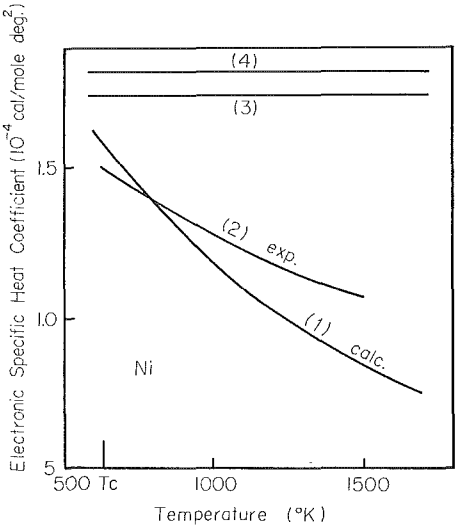

Fig. 33

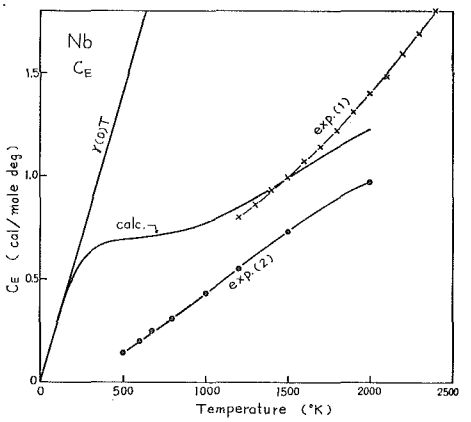

Fig. 34

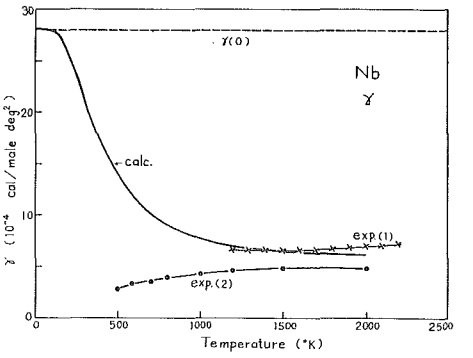

Fig. 35

Fig. 32 Comparison between temperature variations of the calculated and the experimental electronic specific heat for Ni metal. Straight lines (3) and (4) are extrapolations of the low temperature values for ferromagnetic and paramagnetic Ni metal, respectively.

Fig. 33 Comparison between temperature variations of the calculated and the experimental electronic specific heat coefficient for Ni metal. Straight lines (3) and (4) are the low temperature values for ferromagnetic and paramagnetic Ni metal, respectively.

Fig. 34 Comparison between temperature variations of the calculated and the experimental electronic specific heat for Nb metal. Experimental values (1) and (2) are obtained from the data of references 27 and 8, respectively.

Fig. 35 Comparison between temperature variations of the calculated and the experimental electronic specific heat coefficient for Nb metal. Experimental values (1) and (2) are obtained from the data of references 27 and 8, respectively.

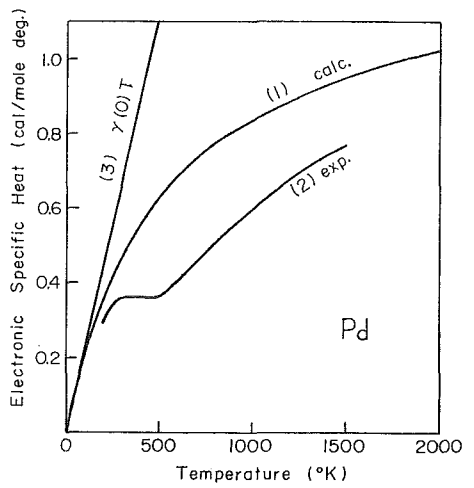

Fig. 36

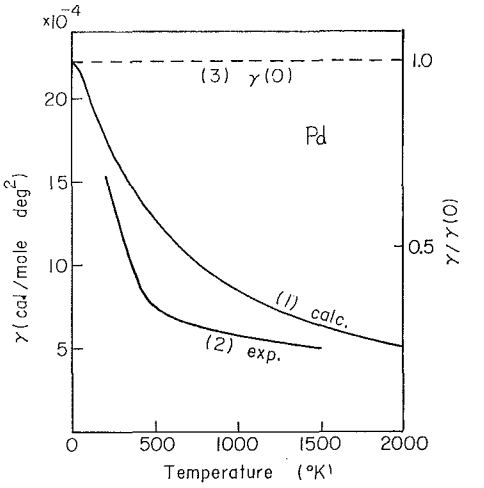

Fig. 37

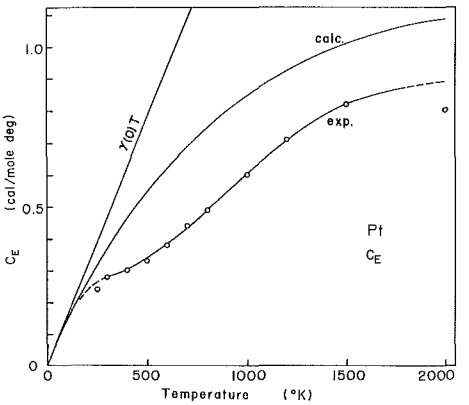

Fig. 38

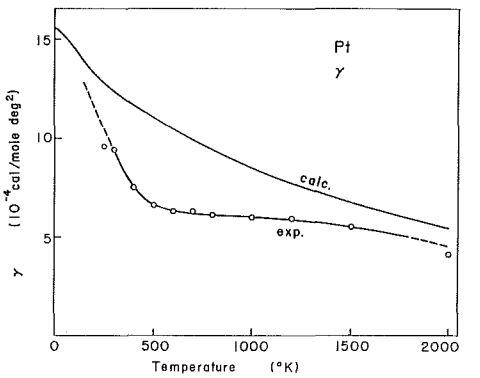

Fig. 39

Fig. 36 Comparison between temperature variations of the calculated and the experimental electronic specific heat for Pd metal.

Fig. 37 Comparison between temperature variations of the calculated and the experimental electronic specific heat coefficient for Pd metal.

Fig. 38 Comparison between temperature variations of the calculated and the experimental electronic specific heat for Pt metal.

Fig. 39 Comparison between temperature variations of the calculated and the experimental electronic specific heat coefficient for Pt metal.

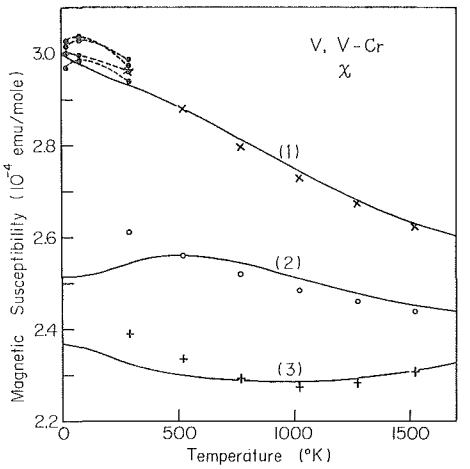

Fig. 40

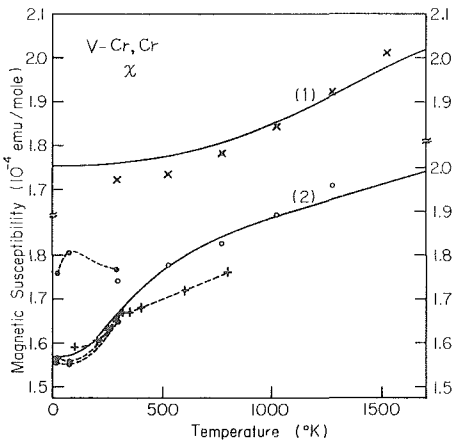

Fig. 41

Fig. 40 Magnetic susceptibilities of V metal and V rich V–Cr alloys.
(1) : calculated result of χ for V metal with $\alpha=0$ and $\chi_c=1.78\times10^{-4}$ emu/mole.
(2) : calculated result of χ for $V_{0.766}$ $Cr_{0.234}$ alloy with $\alpha=0$ and $\chi_c=1.70\times10^{-4}$ emu/mole.
(3) : calculated result of χ for $V_{0.512}$ $Cr_{0.488}$ alloy with $\alpha=0$ and $\chi_c=1.70\times10^{-4}$ emu/mole.
× and ● : observed values of χ for V metal.[28,29]
○ : observed values of χ for $V_{0.75}$ $Cr_{0.25}$ alloy.[30]
+ : observed values of χ for $V_{0.5}$ $Cr_{0.5}$ alloy.[30]

Fig. 41 Magnetic susceptibilities of Cr metal and a Cr rich V–Cr alloy.
(1) : calculated result of χ for $V_{0.259}$ $Cr_{0.741}$ alloy with $\alpha=0$ and $\chi_c=1.45\times10^{-4}$ emu/mole.
(2) : calculated result of χ for Cr metal with $\alpha=0$ and $\chi_c=1.35\times10^{-4}$ emu/mole.
× : observed values of χ for $V_{0.25}$ $Cr_{0.75}$ alloy.[30]
●, ○ and + : observed values of χ for Cr metal.[29,30,31]

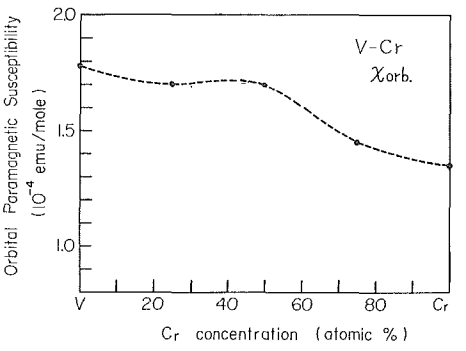

Fig. 42

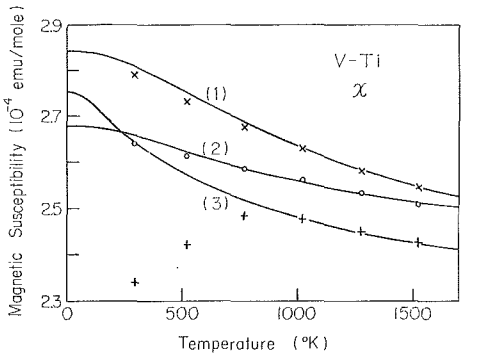

Fig. 43

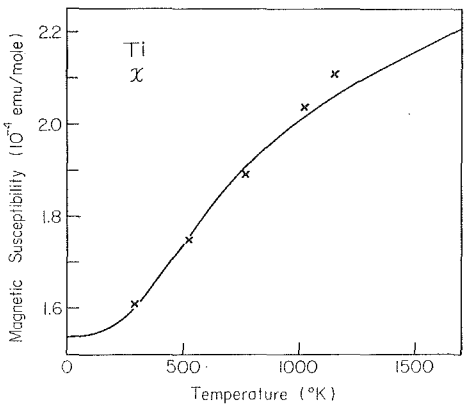

Fig. 44

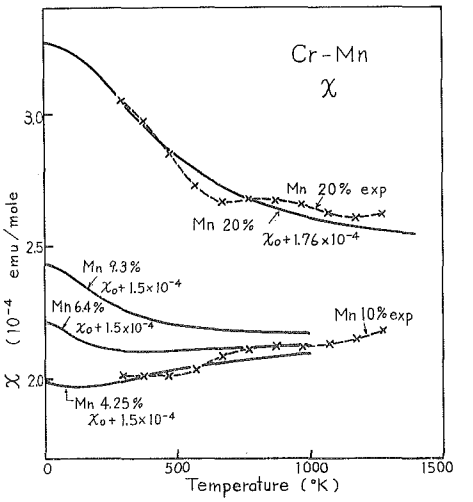

Fig. 45

Fig. 42 Composition dependence of the orbital paramagnetic susceptibility for V–Cr alloys.

Fig. 43 Magnetic susceptibilities of V–Ti alloys.
(1) : calculated result of χ for $V_{0.759}$ $Ti_{0.241}$ alloy with $\alpha = -0.32 \times 10^4$ mole/emu and $\chi_c = 1.85 \times 10^{-4}$ emu/mole.
(2) : calculated result of χ for $V_{0.500}$ $Ti_{0.500}$ alloy with $\alpha = -0.80 \times 10^4$ mole/emu and $\chi_c = 2.00 \times 10^{-4}$ emu/mole.
(3) : calculated result of χ for $V_{0.248}$ $Ti_{0.752}$ alloy with $\alpha = -0.10 \times 10^4$ mole/emu and $\chi_c = 1.70 \times 10^{-4}$ emu/mole.
×, ○ and + : observed values of χ for $V_{0.75}$ $Ti_{0.25}$, $V_{0.5}$ $Ti_{0.5}$ and $V_{0.25}$ $Ti_{0.75}$ alloys, respectively.[30]

Fig. 44 Magnetic susceptibility of Ti metal.
the curve : calculated result of χ for Ti metal with $\alpha = 0.82 \times 10^4$ mole/emu and $\chi_c = 0.73 \times 10^{-4}$ emu/mole.
× : observed valus of χ for Ti metal.[28]

Fig. 45 Magnetic susceptibilities of Cr rich Cr–Mn alloys. Alloys are specified by the atomic concentration of Mn. Experimental values are quoted from reference 30.

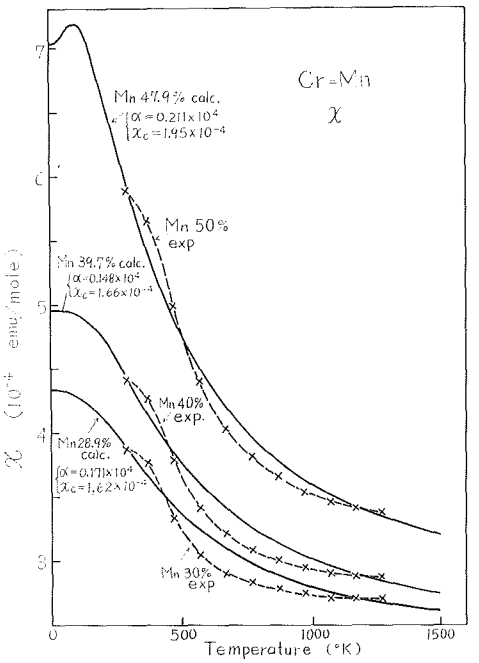

Fig. 46

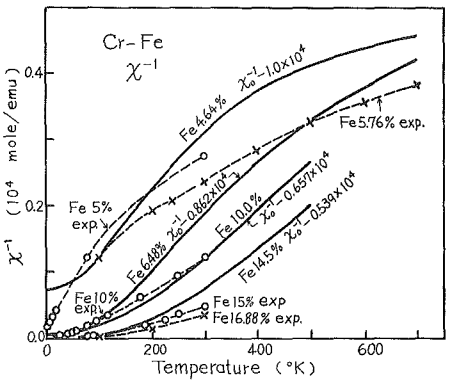

Fig. 47

Fig. 46 Magnetic susceptibilities of Mn rich Cr–Mn alloys. Alloys are specified by the atomic concetration of Mn. Experimental values are quoted from reference 30.

Fig. 47 Reciprocals of the magnetic susceptibilities of Cr–Fe alloys. Alloys are specified by the atomic concentration of Fe. Experimental values, ○ and ×, are quoted from references 33 and 34, respectively.

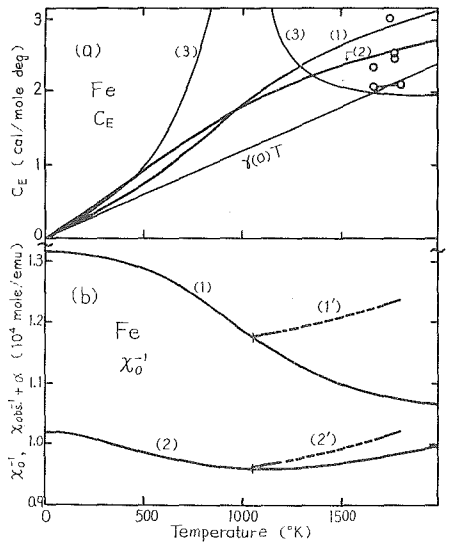

Fig. 48

Fig. 48 Electronic specific heat and magnetic susceptibility for b. c. c. Fe metal.
(a) : Electronic specific heat. Curves (1) and (2) are the calculated results of C_E by using the density of states curves (1) and (2) given in Fig. 49, respectively. Curve (3) and ○'s are experimental values.
(b) : χ_0^{-1} and $\chi_{obs.}^{-1} + \alpha$. Curves (1) and (2) are the calculated results of χ_0^{-1} by using the density of states curves (1) and (2) given in Fig. 49, respectively. Curves (1′) and (2′) are $\chi_{obs.}^{-1} + 1.183 \times 10^4$ mole /emu and $\chi_{obs.}^{-1} + 0.963 \times 10^4$ mole/ emu, respectively.

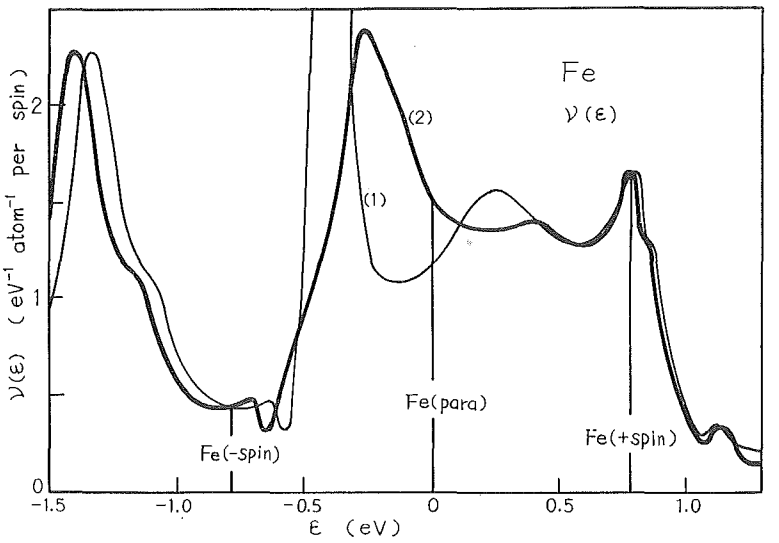

Fig. 49

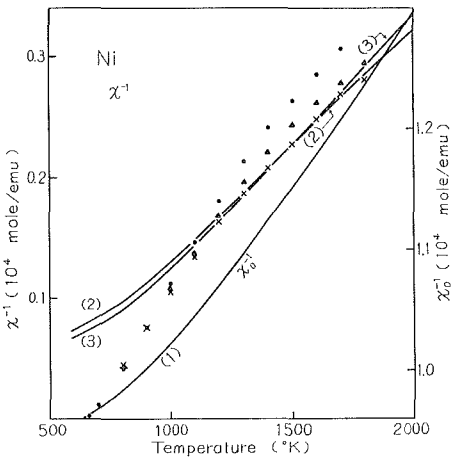

Fig. 50

Fig. 49 Density of states curves for b. c. c. Fe metal.
(1) : the density of states curve given in Fig. 4.
(2) : an improved density of states curve for b. c. c. Fe metal.

Fig. 50 Reciprocal of the magnetic susceptibility of Ni metal.
(1) : calculated result of χ_0^{-1} in right-hand ordinate and $\chi_0^{-1} - 0.96 \times 10^4$ mole/emu in left-hand ordinate.
(2) : calculated result of χ^{-1} with $\alpha = 0.88 \times 10^4$ mole/emu and $\chi_c = 0.71 \times 10^{-4}$ emu/mole.
(3) : calculated result of χ^{-1} with $\alpha = 0.88 \times 10^4$ mole/emu and temperature dependence of χ_c, where $\chi_c = \chi_{c(0)}(1 + 0.903 \times 10^3\ \chi_{spin})^2$ and $\chi_{c(0)} = 0.40 \times 10^{-4}$ emu/mole.
The value of the coefficient 0.903×10^3 has been estimated from spin orbit interaction in Ni atom.
●, × and ▲ : observed values of χ^{-1} for Ni metal.[35,41,42]

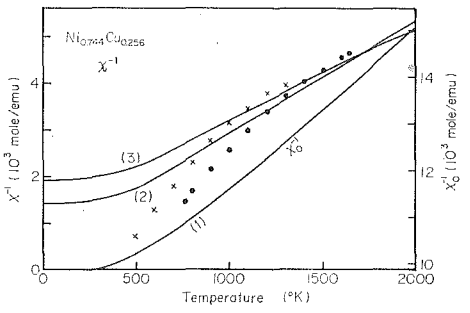

Fig. 51

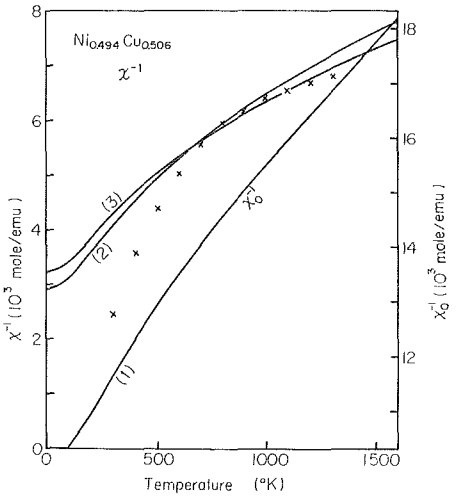

Fig. 52

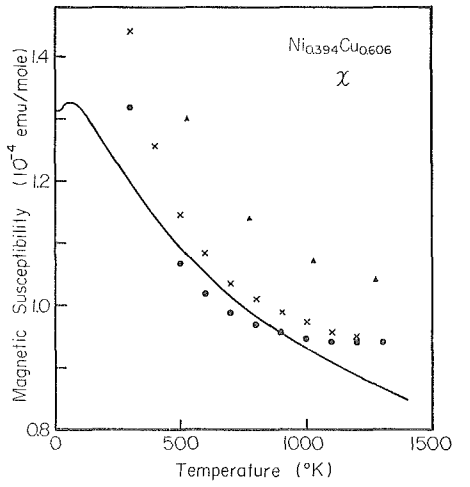

Fig. 53

Fig. 53 Magnetic susceptibility of $Ni_{0.394}Cu_{0.606}$ alloy.
the curve : calculated result of χ with $\alpha = 0.556 \times 10^4$ mole/emu and $\chi_c = 0.2 \times 10^{-4}$ emu/mole for $Ni_{0.394}Cu_{0.609}$ alloy.
●, × and ▲ : observed values of χ for $Ni_{0.386}Cu_{0.614}$ [45] $Ni_{0.41}Cu_{0.59}$ [45] and $Ni_{0.399}Cu_{0.601}$ [43] alloys, respectively.

Fig. 51 Reciprocal of the magnetic susceptibility of $Ni_{0.744}Cu_{0.256}$ alloy.
(1) : calculated result of χ_0^{-1} in right-hand ordinate and $\chi_0^{-1} - 0.986 \times 10^4$ mole/emu in left-hand ordinate, for $Ni_{0.744}Cu_{0.256}$ alloy.
(2) : calculated result of χ^{-1} with $\alpha = 0.829 \times 10^4$ mole/emu and $\chi_c = 0.4 \times 10^{-4}$ emu/mole.
(3) : calculated result of χ^{-1} with $\alpha = 0.762 \times 10^4$ mole/emu and $\chi_c = 0.6 \times 10^{-4}$ emu/mole.
● and × : observed values of χ^{-1} for $Ni_{0.75}Cu_{0.25}$ [42] and for $Ni_{0.731}Cu_{0.269}$ [45] alloys, respectively.

Fig. 52 Reciprocal of the magnetic susceptibility of $Ni_{0.494}Cu_{0.506}$ alloy.
(1) : calculated result of χ_0^{-1} in right-hand ordinate and $\chi_0^{-1} - 1.032 \times 10^4$ mole/emu in left-hand ordinate for $Ni_{0.494}Cu_{0.506}$ alloy.
(2) : calculated result of χ^{-1} with $\alpha = 0.678 \times 10^4$ mole/emu and $\chi_c = 0.4 \times 10^{-4}$ emu/mole.
(3) : calculated result of χ^{-1} with $\alpha = 0.622 \times 10^4$ mole/emu and $\chi_c = 0.5 \times 10^{-4}$ emu/mole.
× : observed values of χ^{-1} for $Ni_{0.491}Cu_{0.509}$ alloy. [45]

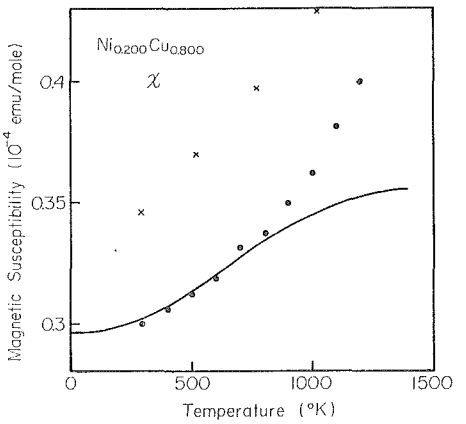

Fig. 54

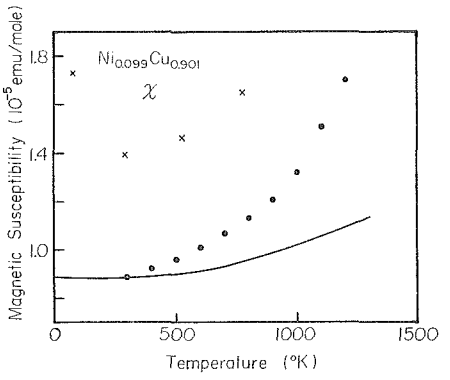

Fig. 55

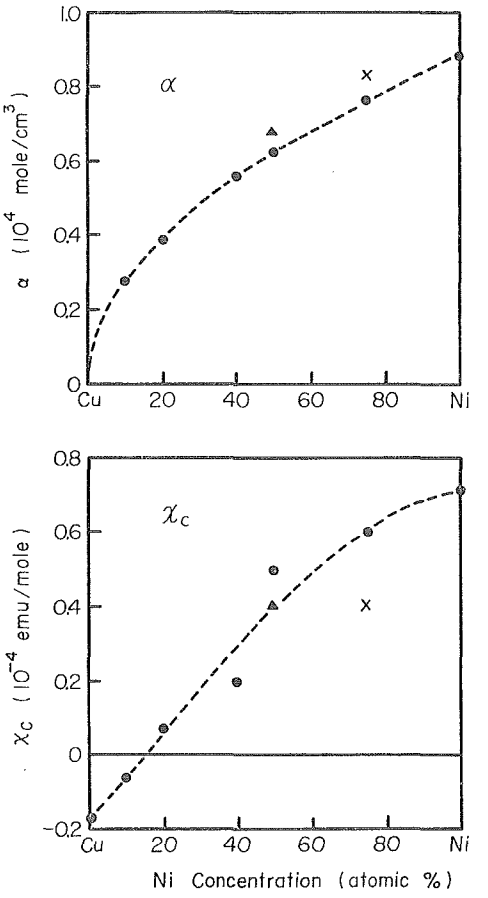

Fig. 56

Fig. 54 Magnetic susceptibility of $Ni_{0.200}$ $Cu_{0.800}$ alloy.
the curve : calculated result of χ with $\alpha = 0.393 \times 10^4$ mole/emu and $\chi_c = 0.07 \times 10^{-4}$ emu/mole for $Ni_{0.200}$ $Cu_{0.800}$ alloy.
● and × : observed values of χ for $Ni_{0.222}$ $Cu_{0.778}$ [45] and $Ni_{0.216}$ $Cu_{0.784}$ [43] alloys, respectively.

Fig. 55 Magnetic susceptibility of $Ni_{0.099}$ $Cu_{0.901}$ alloy.
the curve : calculated result of χ with $\alpha = 0.278 \times 10^4$ mole/emu and $\chi_c = -0.056 \times 10^{-4}$ emu/mole for $Ni_{0.099}$ $Cu_{0.901}$ alloy.
● and × :observed values of χ for $Ni_{0.112}$ $Cu_{0.888}$ [45] and $Ni_{0.118}$ $Cu_{0.882}$ [43] alloys, respectively.

Fig. 56 Composition dependences of the molecular field coefficient, α, and the temperature independent susceptibility, χ_c, in Ni-Cu alloys.

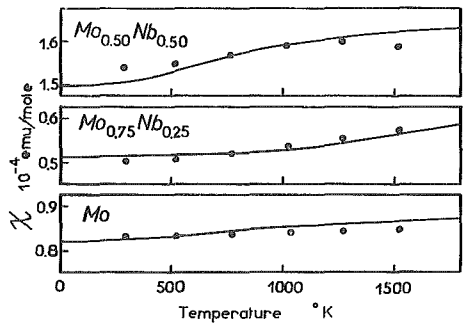

Fig. 57

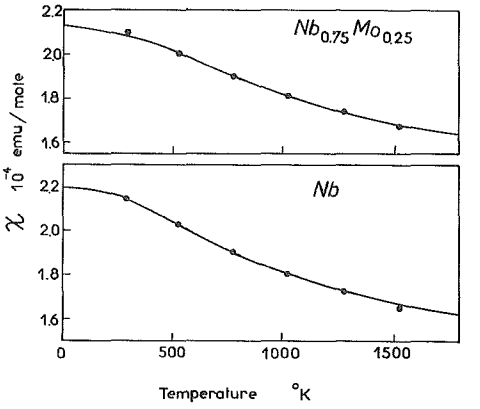

Fig. 58

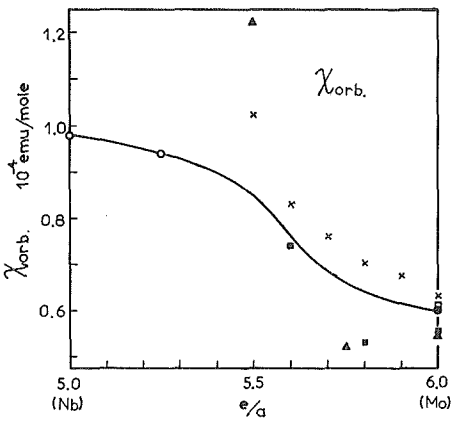

Fig. 59

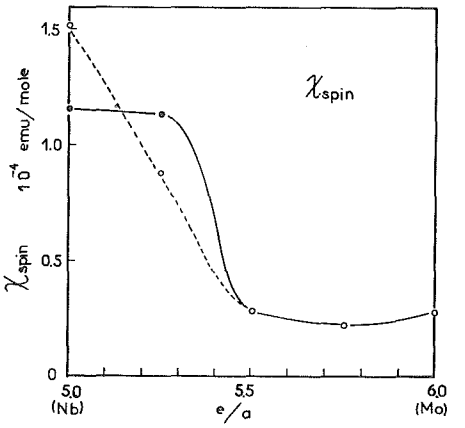

Fig. 60

Fig. 57 Magnetic susceptibilities of Mo metal and Mo rich Nb–Mo alloys.
the curves : calculated results with $\alpha = 0$ and
$\chi_c = 0.544 \times 10^{-4}$ emu/mole for Mo metal,
$\chi_c = 0.521 \times 10^{-4}$ emu/mole for $Nb_{0.25}$ $Mo_{0.75}$ alloy,
$\chi_c = 1.221 \times 10^{-4}$ emu/mole for $Nb_{0.50}$ $Mo_{0.50}$ alloy.
● : observed values.[30]

Fig. 58 Magnetic susceptibilities of Nb metal and a Nb rich Nb–Mo alloy.
the curves : calculated results with
$\alpha = -0.204 \times 10^4$ mole/emu and $\chi_c = 0.980 \times 10^{-4}$ emu/mole for Nb metal,
$\alpha = 0.260 \times 10^4$ mole/emu and $\chi_c = 0.940 \times 10^{-4}$ emu/mole for $Nb_{0.75}$ $Mo_{0.25}$ alloy.
● : observed values.[30]

Fig. 59 Composition dependence of the orbital paramagnetic susceptibility in Nb–Mo alloys.

Fig. 60 Composition dependence of the spin paramagnetic susceptibility in Nb–Mo alloys.

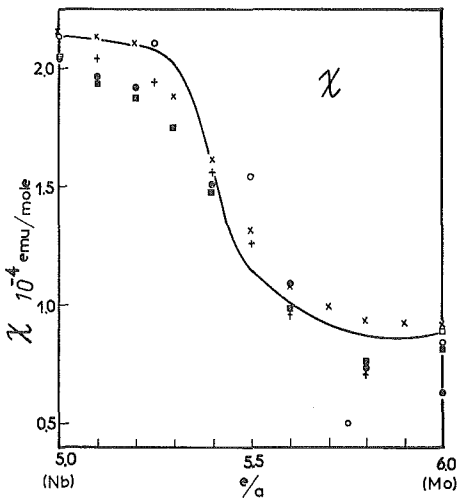

Fig. 61

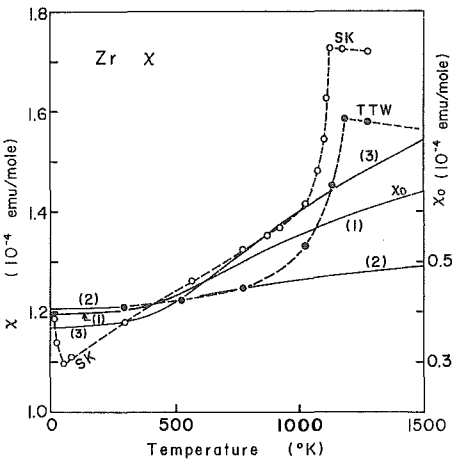

Fig. 62

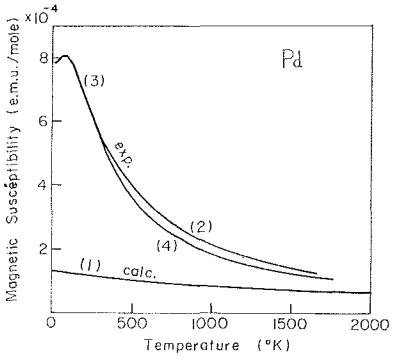

Fig. 63

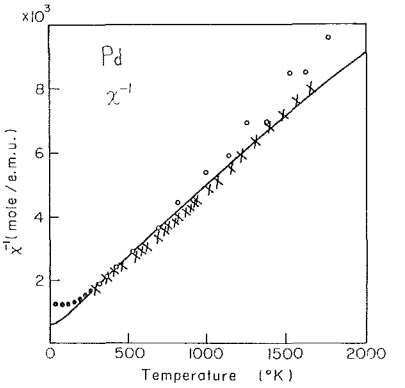

Fig. 64

Fig. 61 Composition dependence of the magnetic susceptibility in Nb–Mo alloys.
the curve : sum of estimated $\chi_{orb.}$ and χ_{spin}.
○, × and ■ : observed values of χ in Nb–Mo alloys.[30,46,47]
● : observed values of χ in Nb–Tc alloys.[49]
+ : observed values of χ in Nb–Re alloys.[46]
□ : observed values of χ in Nb and Mo metals.[48]

Fig. 62 Magnetic susceptibility of Zr metal.
(1) : calculated result of χ_0 in right-hand ordinate and $\chi_0 + 0.8 \times 10^{-4}$ emu/mole in left-hand ordinate.
(2) : calculated result of χ with $\alpha = -1.37 \times 10^4$ mole/emu and $\chi_c = 0.95 \times 10^{-4}$ emu/mole.
(3) : calculated result of χ with $\alpha = 0.37 \times 10^4$ mole/emu and $\chi_c = 0.71 \times 10^{-4}$ emu/mole.
● and ○ : observed values.[30,32]

Fig. 63 Comparison between the calculated result of χ_0 and the experimental results of χ for Pd metal.
(1) : calculated result of χ_0.
(2), (3) and (4) : experimental results of χ.[51,50,28]

Fig. 64 Reciprocal of the magnetic susceptibility for Pd metal. the curve : calculated result of χ^{-1} for Pd metal with $\alpha = 0.724 \times 10^4$ mole/emu and $\chi_c = 0$.
×, ● and ○ : observed values of χ^{-1} for Pd metal.[51,50,28]

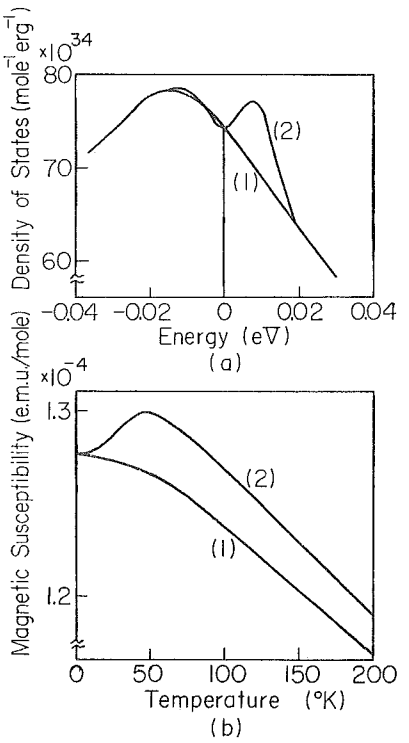

Fig. 65

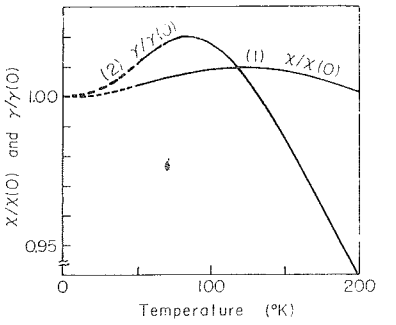

Fig. 66

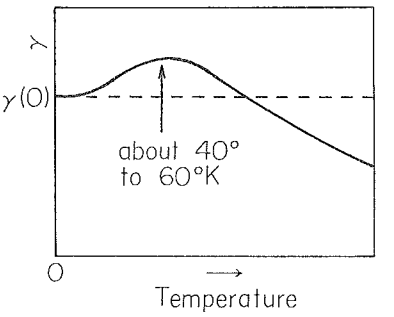

Fig. 67

Fig. 65 A modification of the band shape and the calculated results of χ_0 for Pd metal.
(a) : Band shape. (b) : Calculated results of χ_0.
(1) in (a) : unmodified band shape (just the same as that shown in Fig. 7).
(1) in (b) : calculated result of χ_0 for the unmodified band.
(2) in (a) : a modified band shape.
(2) in (b) : calculated result of χ_0 for the modified band.

Fig. 66 Reduced values of calculated χ_0 and γ for $Pd_{0.9}Ag_{0.1}$ alloy.
(1) : calculated result of $\chi_0/\chi_0(0)$ where $\chi_0(0) = 1.02 \times 10^{-4}$ emu/mole.
(2) : calculated result of $\gamma/\gamma(0)$ where $\gamma(0) = 17.7 \times 10^{-4}$ cal/mole deg^2.

Fig. 67 Schematic diagram for the expected anomaly in γ of Pd metal.

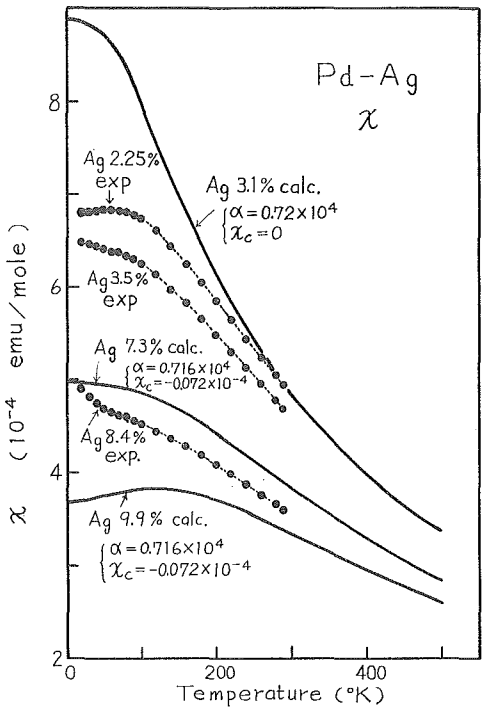

Fig. 68

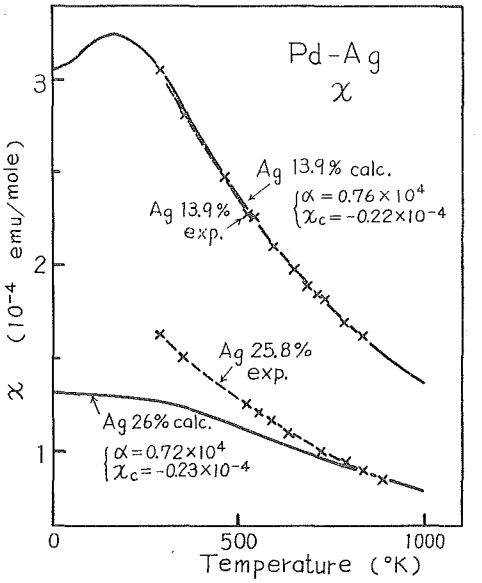

Fig. 69

Fig. 68 Magnetic susceptibilities of Pd–Ag alloys. Experimental values, ●, are quoted from reference 9.

Fig. 69 Magnetic susceptibilities of Pd–Ag alloys. Experimental values, ×, are quoted from reference 51.

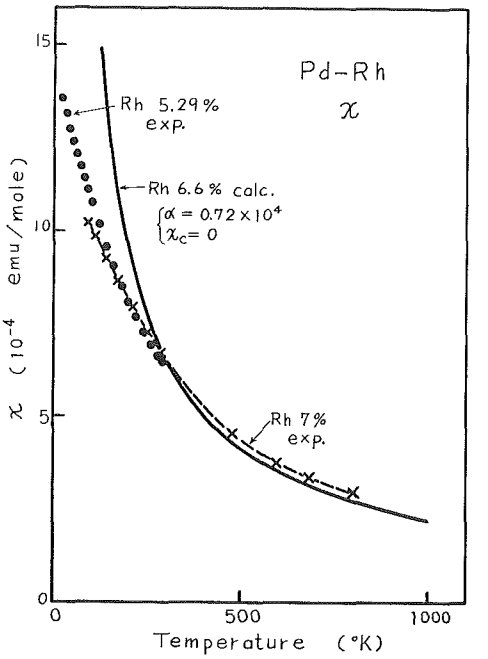

Fig. 70

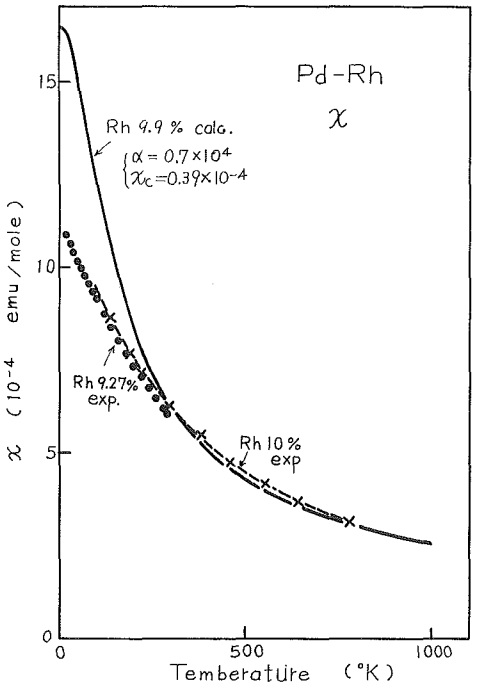

Fig. 71

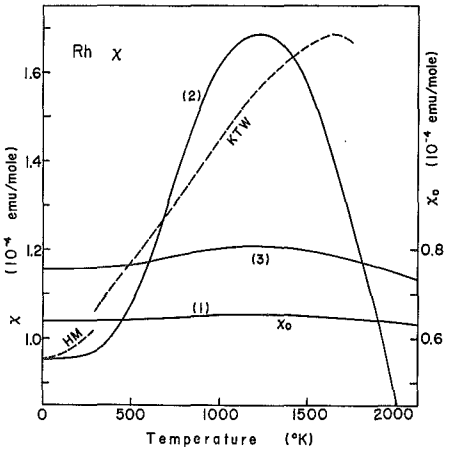

Fig. 72

Fig. 70 Magnetic susceptibilities of Pd–Rh alloys. Experimental values, ● and ×, are quoted from references 22 and 54, respectively.

Fig. 71 Magnetic susceptibilities of Pd–Rh alloys. Experimental values, ● and ×, are quoted from references 22 and 54, respectively.

Fig. 72 Magnetic susceptibility of Rh metal.
(1) : calculated result of χ_0 in the right-hand ordinate and $\chi_0 + 0.4 \times 10^{-4}$ emu/mole in the left-hand ordinate.
(2) : calculated result of χ with $\alpha = 1.33 \times 10^4$ mole/emu and $\chi_c = -3.22 \times 10^{-4}$ emu/mole.
(3) : calculated result of χ_{spin} with $\alpha = 0.7 \times 10^4$ mole/emu.
dashed curves : experimental results.[50,28]

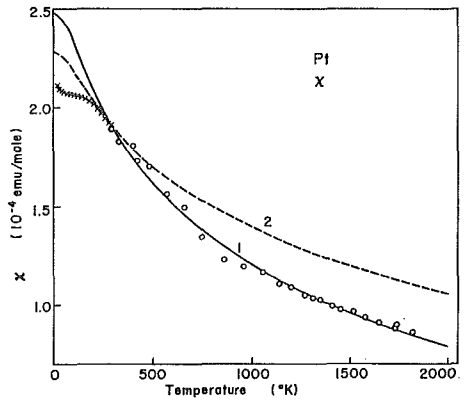

Fig. 73

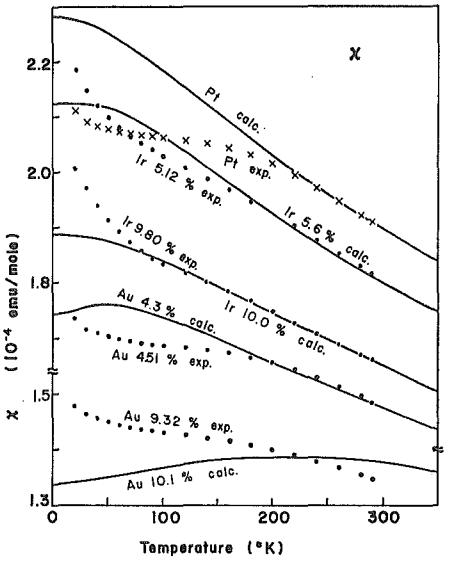

Fig. 74

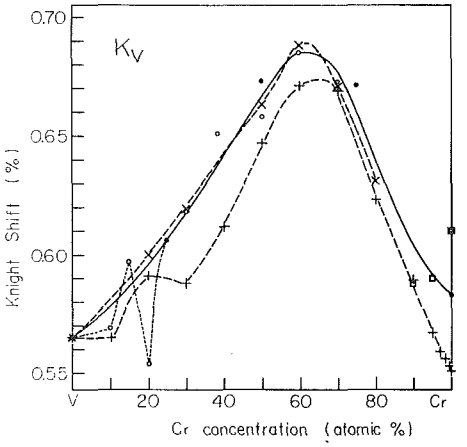

Fig. 75

Fig. 75 NMR shifts of V^{51} in V metal and V–Cr alloys. ○, ● and □ are calculated values by making use of the observed values of χ given in references 29, 30 and 31, respectively, and the values of parameters, $c = 52$ mole/emu and $b' = -30.6$ mole/emu. + and × are observed values.[57,58] The solid line is obtained by smoothly joining the calculated points. The oscillation of the calculated values in V rich region arises from the oscillation of the observed value of χ.[29]

Fig. 73 Magnetic susceptibility of Pt metal.
(1) : calculated result of χ with $\alpha = 0.74 \times 10^4$ mole/emu and $\chi_c = -0.15 \times 10^{-4}$ emu/mole.
(2) : calculated result of χ with $\alpha = 0.64 \times 10^4$ mole/emu and $\chi_c = 0.2 \times 10^{-4}$ emu/mole.
× and ○ : observed values.[22,28]

Fig. 74 Magnetic susceptibilities of Pt metal, Pt–Ir alloys and Pt–Au alloys. Alloys are specified by the atomic concentration of Ir or Au. Calculated results of χ are obtained with following values of parameters :
$\alpha = 0.64 \times 10^4$ mole/emu and $\chi_c = 0.2 \times 10^{-4}$ emu/mole for Pt metal,
$\alpha = 0.63 \times 10^4$ mole/emu and $\chi_c = 0.01 \times 10^{-4}$ emu/mole for Au 4.3% alloy,
$\alpha = 0.62 \times 10^4$ mole/emu and $\chi_c = 0.01 \times 10^{-4}$ emu/mole for Au 10.1% alloy,
$\alpha = 0.59 \times 10^4$ mole/emu and $\chi_c = 0.19 \times 10^{-4}$ emu/mole for Ir 5.6% alloy,
$\alpha = 0.60 \times 10^4$ mole/emu and $\chi_c = 0.04 \times 10^{-4}$ emu/mole for Ir 10.0% alloy.
Experimental values are quoted from reference 22.

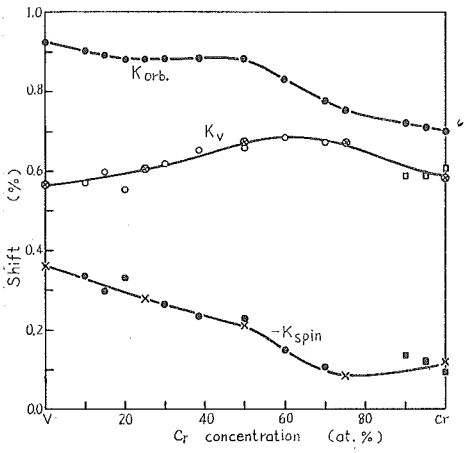

Fig. 76

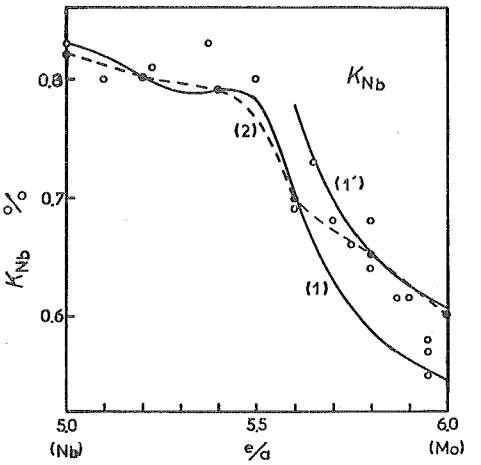

Fig. 77

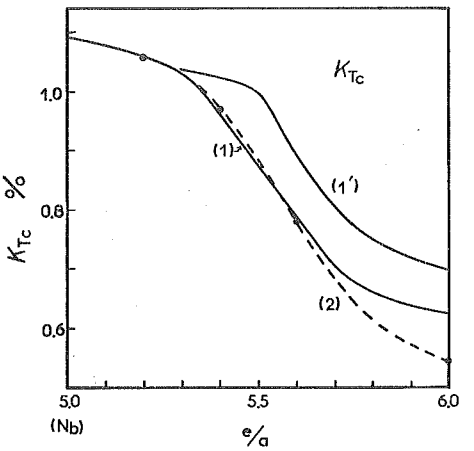

Fig. 78

Fig. 76 NMR shift of V^{51} in V metal and V–Cr alloys, K_V, and contributions from the orbital paramagnetism, $K_{orb.}$, and from the exchange polarization and the hyperfine interaction, K_{spin}.

Fig. 77 NMR shift of Nb^{93} in Nb–Mo and Nb–Tc alloys.
(1) : calculated result with $c = 95$ mole/emu and $b' = -8.71$ mole/emu.
(1′) : calculated result with $c = 105$ mole/emu and $b' = -8.71$ mole/emu.
○ : observed values in Nb–Mo alloys under $H = 15$ KOe.[62]
● and (2) : observed values in Nb–Tc alloys under $H = 14$ KOe.[49]

Fig. 78 NMR shift of Tc^{99} in Nb–Tc alloys.
(1) : calculated result with $c = 100$ mole/emu and $b' = +9.45$ mole/emu.
(1′) : calculated result with $c = 120$ mole/emu and $b' = -7.17$ mole/emu.
● and (2) : observed values under $H = 14$ KOe.[49]

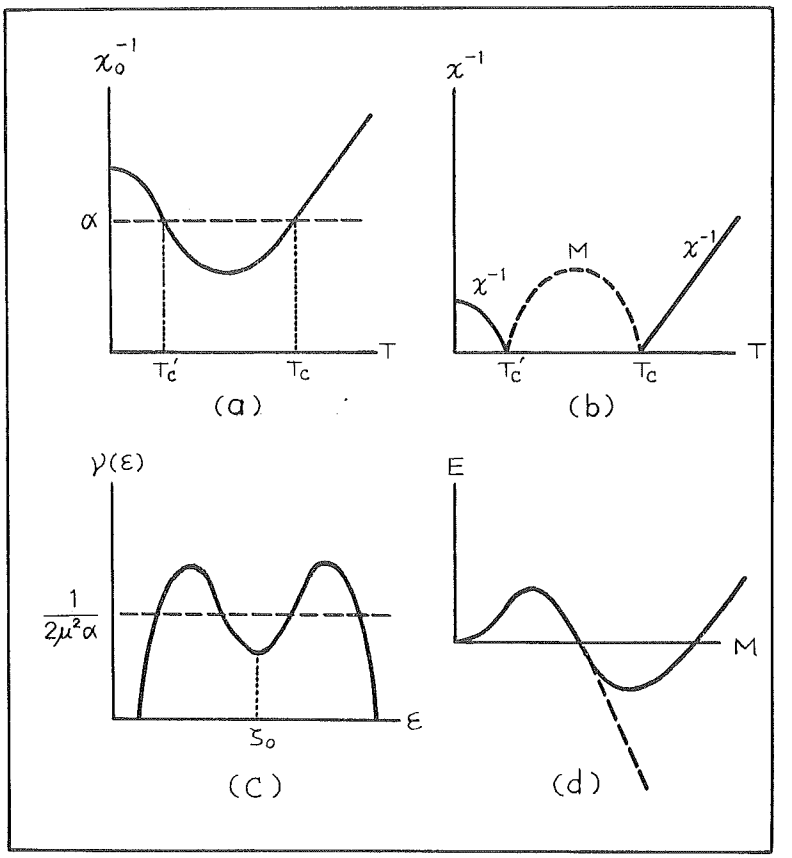

Fig. 79

Fig. 79 Schematic diagrams.

(a) : Temperature variation of the reciprocal of the spin paramagnetic susceptibility without molecular field, χ_0.

(b) : Temperature variations of the reciprocal of the spin paramagnetic susceptibility with molecular field (full lines) and of the magnetization (broken line).

(c) : Density of states when χ_0 varies with temperature as shown in (a).

(d) : Total energy E as a function of M.